Subregional activity in the dentate gyrus is amplified during elevated cognitive demands

Charlotte C.M. Castillon[1], Shintaro Otsuka[1], John N. Armstrong[1], Anis Contractor[1,2,3]

[1]Department of Neuroscience, [2]Department of Psychiatry and Behavioral Sciences Feinberg School of Medicine, [3]Department of Neurobiology, Weinberg College of Arts and Sciences Northwestern University

Correspondence: Anis Contractor
Dept of Neuroscience
Northwestern University Feinberg School of Medicine
303 E. Chicago Ave
Chicago, Il 60611
a-contractor@northwestern.edu
Tel: 312 503 1843

Words in Abstract – 265 ; Introduction – 468 ; Discussion - 1282

Acknowledgements: We thank members of the Contractor lab for helpful discussion and Ms. Astrid Castellanos for assistance during the performance of this study. This work was supported by NIH/NINDS 5R01NS115471 to AC.

Author Contributions: C.C.M.C., J.N.A., and A.C. designed experiments. C.C.M.C. performed all behavioral testing, immunohistochemistry, imaging and analysis. S.O. developed the touch screen automated task and produced code to operate the procedures. C.C.M.C. and A.C. prepared the manuscript. All authors approved the final version.

Abstract:

Neural activity in the dentate gyrus (DG) is required for the detection and discrimination of novelty, context and patterns, amongst other cognitive processes. Prior work has demonstrated that there are differences in the activation of granule neurons in the supra and infrapyramidal blades of the DG during a range of hippocampal dependent tasks. Here we used an automated touch screen pattern separation task combined to temporally controlled tagging of active neurons to determine how performance in a cognitively demanding task affected patterns of neural activity in the DG. We found an increase in the blade-biased activity of suprapyramidal mature granule cells (mGCs) during the performance of a high cognitive demand segment of the task, with a further characteristic distribution of active neurons along the apex to blade, and hilar to molecular layer axes. Chemogenetic inhibition of adult-born granule cells (abDGCs) beyond a critical window of their maturation significantly impaired performance of mice during high-demand conditions but not when cognitive demand was low. abDGC inhibition also elevated the total activity of mGCs and disturbed the patterned distribution of active mGCs even in mice that eventually succeeded in the task. Conversely chemogenetic inhibition of mGCs reduced success in the high cognitive demand portion of this task and decreased the global number of active GCs without affecting the patterned distribution of active cells. These findings demonstrate how a high cognitive demand pattern separation task preferentially activates mGCs in subregions of the DG and are consistent with a modulatory role for abDGCs on the dentate circuit which in part governs the spatially organized patterns of activity of mGCs.

Introduction:

The dentate gyrus (DG) is the input structure to the hippocampus and plays important roles in episodic memory [1], spatial coding [2], novelty detection [3] as well as in separating patterns [4]. In addition to the local circuit composed of granule cells and interneurons, the neurogenic niche in the subgranular zone (SGZ) of the DG gives rise to the generation of adult-born granule cells (abDGCs) [5-8], which has been of significant interest for its potential to reorganize hippocampal microcircuits and contribute to memory flexibility [9].

While multiple functions have been ascribed to the DG, a long-standing proposal stems from early computational studies that inferred a role in pattern separation based on the anatomical connectivity of the DG [10-12] . The DG is the gateway to the hippocampus receiving direct excitatory input from the entorhinal cortex (EC). The large number of granule neurons in the DG receiving input from a relatively smaller population of EC has been proposed to allow expansion

recoding which, along with sparse firing of granule cells, allows the separation of inputs at the level of neural activity [13].

Prior work has demonstrated that mature granule cells (mGCs) localized in the two blades of the dentate gyrus termed suprapyramidal (SB) and infrapyramidal (IB) when viewed in transverse cross section [14], have an asymmetric biased activation [15-18]. More mGCs in the SB are engaged during hippocampal dependent tasks than those in the IB [15,17,18]. The precise roles of abDGCs versus mGCs in DG function remain unclear, and a circuit-based explanation for the observed bias in mGC activity is still lacking. The divergence in mGC activity across the blades of the DG is paralleled in the asymmetry of neurogenesis in the DG with elevated numbers of adultborn dentate granule cells (abDGCs) observed in the neurogenic niche of the SB [19-22]. In this study we examined whether performance in a cognitively demanding task affected the patterns of neural activity in the dorsal DG and whether abDGCs played a role in this process. To do so, we used TRAP2 mice [23] for temporally defined labeling of active neurons, we confirmed that both mGCs and abDGCs were engaged during an automated spatial discrimination task. When the cognitive demand of the task was elevated by reducing the degree of spatial separation, there was an increase of mGC activity and a more prominent and amplified spatial bias with active neurons distributed preferentially to the SB and relatively reduced in the IB. Chemogenetic inhibition of abDGCs during the task decreased performance in the task. Importantly, the overall number of active mGCs was increased and the blade-biased distribution was significantly reduced suggesting that the task specific mGC neural representation are disrupted by inhibiting activity of abDGCs. Together, these findings reinforce the significance of neural activity in the dorsal DG in spatial pattern separation and highlight the circuit contributions of both abDGCs and mGCs to behaviors requiring a high cognitive demand.

Results:

Blade-biased activity of GCs during a high cognitive demand pattern separation task

Prior work has demonstrated that expression of immediate early genes in the DG including Arc [15], c-Fos [18] and Zif268 [24] correlate with behavioral state and are active in both mature and young abDGCs. Genetic strategies using TRAP1 mice [25] and TetTag mice [26,27] have also demonstrated that active GC populations can be labeled with these strategies. To determine whether behaviorally induced labeling of both mGCs and abDGCs is observed in TRAP2 mice ($Fos^{2a\text{-}iCreERT2}$;Ai9) we combined birth-dating of abDGCs with a single exposure to voluntary wheel running which is known to activate DG neurons [25] (Figure S1A). Mice given access to running wheels for 4 hours had elevated numbers of TRAP+ neurons throughout the DG, with both mature and immature neurons labeled (Figure S1B-F). TRAP+ labeling of abDGCs was

observed in birth-dated neurons 14 days post injection (dpi) from BrdU (Figure S1E & F). No double labeled TRAP+ BrdU+ neurons were observed in younger neurons prior to this timepoint (Figure S1F). Importantly, an analysis of the blade specific localization of TRAP+ neurons demonstrated that in home cage controls there was a small bias in the distribution of active neurons to the SB of the DG and this distribution of labeled GCs was not different in mice exposed to a single episode of running (Figure S1D).

In order to determine the activation patterns of GCs when mice successfully performed a high cognitive demand spatial discrimination pattern separation task, TRAP2 mice were trained in a modified touch screen task that tests the ability to separate a unique pattern of illuminated squares posing a relatively low or high cognitive demand (Figure 1A and Figure S2A & B). The trial unique nonmatching-to-location (TUNL) task has been demonstrated to require the hippocampus, particularly when the cognitive demand is high when the separation of the sample to test squares is reduced, or the delay between sample and choice is increased [28,29]. Mice were injected with BrdU to birthdate neurons at day 0 (D0). At D7 mice were water restricted before EdU injections and shaping at D14 to habituate them to the operant task and learn to touch the screen for a saccharine water reward. Mice were then trained until they reached criterion (70% correct during one of two daily sessions on 2 consecutive days) in the TUNL task with a 1s delay between the sample and choice and a large (L) separation between sample panel and the test panel (Figure 1A and Figure S2A). Mice reached criterion on average at 10.7 ± 0.8 days in the large separation sessions (Figure 1B & D left panel). After reaching criterion the mice were tested with alternating trials of large and small (LS) separation between the sample and test panels. In this case the mice were always above criterion for the L trials but took another 9.3 ± 1.0 days to reach criterion on the S trials (Figure 1C & D middle and right panel).

Different cohorts of mice were analyzed at each stage to determine the extent of TRAPed cells in the DG along with labeling for thymidine analogs which birth-dated the abDGCs at approximately 3 weeks (25 ± 1.4 days) for EdU and 5 weeks (39 ± 1.2 days) for BrdU (Figure 1E). We found a strong relationship between the stage of training in the task and the degree of activation of the mGCs with more TRAP+ neurons in mice after the completion of the L separation than during shaping, and the greatest density of TRAP+ neurons in mice engaged in the high cognitive demand task (LS) (Shape – LS, $p = 0.007$)(Figure 1F), regardless of whether the mice reach the criterion (C) or not (NC)(Figure S2G). Furthermore, when we examined the correlation between successful performance to criterion and the number of TRAP+ neurons, we

found no significant relationship (Figure S2C), demonstrating that increased DG activity is driven by engagement in a high-demand task rather than task success.

In the two cohorts of abDGCs that were birth-dated by BrdU and EdU we observed TRAP+ cells with only a low abundance. Approximately 1% of 25- to 39-day-old abDGCs were active (TRAP+) during the pattern separation task (LS) (Figure 1G), regardless of whether the mice reached the criterion (C) or not (NC)(Figure S2I). In contrast, in mice that only performed the low cognitive demand task (L configuration only) we observed almost no TRAP+ labeled birth-dated cells (Figure 1G). In a final group of mice, we TRAPed neurons in mice on the final day of LS trials. Mice were then reintroduced to the task (LS) 3 days later for two sessions on a single day before being perfused for immunohistochemical analysis of endogenous c-Fos expression (90 min after behavior, Figure 1A). Performance of mice in the task was diminished compared to the last day of prior training in both the L and S trials (Figure 1D, middle panel). Assessment of re-activation of mGCs (i.e., TRAP+ cells expressing endogenous c-Fos after the last session) was measured in these mice, with a larger overlap in TRAP+/c-Fos+ cells for mice who performed the LS trials than in mice that only performed L separation trials ($p = 0.05$) (Figure 1H). Collectively, our results demonstrate that performing a high cognitive demand task of visual pattern separation increases the activation of DG granule cells including both mGCs and abDGCs.

To determine whether performance of the high cognitive demand pattern separation task altered the spatial profile of active mGCs we conducted an analysis of the spatial distribution of TRAP+ mGCs in the DG (Figure 2). After performing the high cognitive demand LS task there was a marked spatial bias of TRAP+ cells in mice with active neurons distributed preferentially to the SB than the IB in the DG. This spatial bias was driven by both an increase in the number of labeled cells in the SB and a decrease in the IB ($p= 0.0282$) (Figure 2A & S2E). However, as with overall TRAP+ cell density, we found no significant correlation between task performance and the percentage of TRAP+ neurons in the SB (Figure S2D). A further analysis of active neurons in the DG (TRAP+) to determine the location in relation to the hilus and dentate apex demonstrated that active cells were more prominent in the outer radial areas of the granule cell layer (GCL) a region that has an enrichment in spatially biased semilunar granule cells [17,30], and closer to the DG apex in mice after the more demanding LS task (Figure 2B & C). These data demonstrate that the biased activity of suprapyramidal granule neurons is amplified during the high cognitive demand segment of the TUNL task compared to lower-demand tasks (Figure

S2E). In high demanding tasks, there is also a pronounced difference in the distribution of the active neurons along the apex to distal blade and the hilar to outer GCL axes (Figure 2D & E).

Activation of GCs during remote recall in the high cognitive demand task

We next investigated whether a similar spatially biased activity of GCs was observed in a remote recall (R) test three weeks after reaching the criterion during the initial training (I), and whether there was overlap in the population of active DG neurons (Figure 3A). In the remote session, mice had a high success rate performing close to criterion in the L trials on the first day of retesting suggesting that 3 weeks after initial learning they retained the ability in task (Figure 3B). However, when confronted with the more demanding trials with inclusion of the small separation configuration, mice required additional days to achieve the criterion level (Figure 3C), although most mice required less time to reach criterion in LS training during the remote trials than on the initial testing (Figure 3D). We again observed that the density of TRAP+ cells was increased in mice that underwent LS compared to L only trials during the initial training (not shown) and importantly the distribution of active neurons during both the initial training (TRAP+) and remote training (c-Fos+) were biased to the SB after LS training (Figure 3F & G).

An analysis of birth-dated active neurons labeled during the initial training (TRAP+) or during the remote trials (c-Fos+) demonstrated a small number of BrdU (~4 weeks) neurons were labeled during the initial training (Figure 3H) whereas in the remote training we observed both BrdU labeled (7.7 weeks) and EdU labeled (5.7 weeks) abDGCs that were c-Fos+ only in mice after LS training (Figure 3I). No birth-dated abDGCs were found that were double labeled TRAP+ and c- Fos+, however we observed dual labeled mGCs with more TRAP+/c-Fos+ labeled neurons in mice that had performed LS training than those that only performed L training ($p=0.0433$) (Figure 3J).

Taken together, these results demonstrate that during initial training and remote training in the pattern separation task, spatially biased activity of neurons is observed in the SB but there is little overlap in activity of neurons in the DG of mice during these epochs of training.

DREADD inhibition of abDGCs disrupts blade-biased activity of mGCs and performance of mice in a high cognitive demand task

abDGCs are known to affect the excitability of mGCs [31,32] and there is a demonstrated blade bias in neurogenesis in the DG. However, it remains unknown whether abDGCs affect the blade-biased activity patterns of mGCs that are evident during a pattern separation task. To acutely modulate the activity of abDGCs during task performance, we created mice in which the

inhibitory DREADD (designer receptor exclusively activated by designer drugs) could be conditionally expressed in abDGCs by crossing R26-LSL-Gi-DREADD mice (hM4Di) [33] to Ascl1^{CreERT2} mice. This selectively expresses the hM4Di inhibitory DREADD in a birth-dated cohort of abDGCs by the delivery of TAM (tamoxifen, see Methods) in the diet of mice for 7 weeks allowing the inhibition of their activity with a selective ligand deschloroclozapine (DCZ)(50 μg.kg^{-1})[34] during the LS sessions of the task (Figure 4A & B) [35,36]. Inhibition of abDGCs (≤ 7 weeks old) using the DREADD ligand DCZ increased the time animals took to reach criterion compared control groups of animals that received DMSO or were Cre negative (Cre-) ($p = 0.01$ and $p = 0.05$) (Figure 4C & D). This impairment was specific to the cognitively more demanding LS task, as inhibiting ≤ 7-week-old abDGCs did not affect the performance of mice once they had learned the L configuration (not shown). Importantly control groups that had also received TAM in their diet showed no effect in the pattern separation task or in the biased blade activity of mGCs (Figure 4C-J). Taken together this experiment suggests that abDGCs in this cohort (≤ 7 weeks) are beneficial to performance in a pattern separation task.

Prior work has demonstrated that abDGC loss causes an increase in activity of mGCs [31,37] which is likely through a loss of connections to hilar interneurons which provide feedback inhibition to the DG. Consistent with this, analysis of c-Fos in the DG demonstrated increased labeling across the DG when abDGCs were inhibited with DCZ activation of hM4Di compared to control groups ($p=0.0271$) (Figure 4E & F). Conversely, c-Fos+ labeling in the downstream CA3 region of the hippocampus demonstrated no significant difference in density between the control groups and abDGC inhibition (Figure 4G). Interestingly, we found that the biased distribution of c-Fos+ neurons in the two control groups showed the same profile as we had observed before in the IB and SB after mice perform the high cognitive demand task (Figure 4H). However, in the cohort of mice in which abDGCs were inhibited, the prominent biased distribution pattern of activity was not observed ($p = 0.01$) (Figure 4H). Furthermore, the distribution of c-Fos+ cells within the blades showed that when abDGCs were inhibited during LS training there was a marked prominence of labeled neurons located near the hilus in both the IB and SB in the region closest to the subgranular zone (SGZ), the neurogenic niche of the DG where abDGCs are produced, raising the possibility that these neurons are under greater feedforward inhibitory control via abDGCs (Figure 4I). In summary, DREADD inhibition of ≤ 7-week-old abDGCs during the LS high cognitive demand task resulted in a reduction in both in biased SB-IB spatial activity pattern as well as the activity labeling of neurons along both axes of the transverse DG (Figure 4J), and this altered activity correlated with a reduction in performance of animals which required increased days to complete the high cognitive demand task.

In the previous experiments we provided TAM to mice in their diet to cause expression of hM4Di in neurons that range from 0 days to 7 weeks. This covers abDGCs that are within their critical period when they demonstrate strong plasticity and excitability and are well connected to the hippocampal network [38,39]. To determine if DREADD inhibition of a population of younger neurons had any effect on the pattern separation task we supplied TAM in the diet for 4 weeks to express hM4Di in abDGCs ≤ 4 weeks (Figure 5A). In the LS high cognitive demand task, there was no difference in the time to criterion of animals that had received DCZ administration for hM4Di inhibition of abDGCs compared to the control groups (Figure 5B). Similarly, analysis of c-Fos+ density in the DG found no difference in overall density (Figure 5C) and the blade distribution of active mGCs after hM4Di (Figure 5D) or in the hilar to molecular layer axes distribution (Figure 5 E).

Taken together these results demonstrate that ≤ 7-week-old cohort of abDGCs that include neurons in their critical period of development influence the excitability and spatially biased pattern of activity of mGCs in the DG and also affect the performance of mice in a high cognitive demand pattern separation task. In contrast young neurons at ≤ 4 weeks do not influence either the performance of mice in the task or the spatial distribution of activity in the DG.

Both the increase of mGC activity and the blade-biased distribution are necessary to perform in high cognitive demand task.

Our results have confirmed that the activity of mGCs, which can be regulated by abDGCs, is required for the efficient performance in a high cognitive demand pattern separation task. mGCs are under strong inhibitory control and are sparsely active in vivo [40,41]. To assess how artificially affecting their activity with an inhibitory DREADD we crossed Dock10-Cre mice [42] with R26-LSL-Gi-DREADD mice to express the hM4Di in mGCs and assessed their performance in the high cognitive demand task (Figure 6C). We first examined Dock10-Cre expression in newborn neurons (BrdU+) and found relatively few 2-week-old neurons with increasing numbers of double labelled abDGCs weeks postmitosis, in non-DCX positive neurons (Figure S3), reaching 80% of abDGCs after 7 weeks (Figure 6A & B), demonstrating that Dock10-Cre is expressed principally in mGCs and older abDGCs. As we had predicted, DREADD inhibition of mGCs caused a majority of mice to not succeed in reaching criterion (62.5%) within the 14 day LS cutoff we imposed compared to mice in the control group (34.8%)(p=0.0452)(Figure 6D & E). Performance in the interleaved low demand L trials was not degraded by mGC DREADD inhibition (not shown). There was a clear reduction in total c-Fos+ labeling in the DG (p = 0.04) and CA3 (p = 0.006) of mice that did not achieve criterion after 14 days (Figure 6F, G & I).

Surprisingly, despite mice not reaching criterion in the LS task and reduced overall activity there was a biased distribution of active c-Fos+ labeled neurons to the SB which was no different to control mice that reached criterion, suggesting that both the overall excitability and biased distribution of mGC activity are essential for a high cognitive demand pattern separation task (Figure 6H, J & K).

Discussion:

In this study we used activity labeling techniques combined with a complex, automated visual spatial pattern separation task to capture patterns of activity of GCs in the dorsal DG. The DG is a critical part of the hippocampal formation that receives extrinsic input from cortex and other structures but is also highly regulated by local connections with hilar and CA3 neurons[13]. While many roles have been ascribed to the dorsal DG, a prominent theory has been that its activity is vital to pattern separation [43]. We found that activity labeling of neurons demonstrated unique spatial distributions of active GCs which were amplified when the separation task was made more stringent for the mice. In particular, we observed a biased distribution of active neurons in the SB, which was elevated in mice that completed the LS task. There have been prior descriptions of a blade-biased distribution of active neurons when mice engage in hippocampal dependent behaviors [15-18] however it is still not known how these spatially defined activity patterns are modulated or established. We found that not only is there a bias towards more activity in SB and less in the IB during a more demanding task, there is also an increase in activity density in the outer radial areas of the granule cell layer (GCL) where semilunar granule cells are enriched [17,30], and in regions closer to the dentate apex. These elevated biased spatial distributions of active neurons were not observed when mice were assessed after running or after the low cognitive demand version of the task, two behaviors that increases activity of mGCs significantly but do not enhance their blade-biased distribution (Figure S2E). However, while blade-specific differences in activity are evident, no distinct, independent microcircuit has been identified that exclusively governs the function of either the SB or IB. This raises an important question as to whether these differences arise solely from variations in afferent connectivity and intrinsic GC properties or if they reflect an underlying, segregated network organization within the DG. Future studies exploring whether the SB and IB operate as distinct computational units or as interconnected components of a larger network will be essential to clarify the functional basis of this observed bias.

abDGCs in dentate function

The dentate gyrus also, uniquely for a temporal lobe structure, has a neurogenic niche where new neurons are born and integrate into the existing network in the dentate. Post mitotic abDGCs develop over the course of several weeks [44], reaching maturity by around 8 weeks post mitosis where their functional properties and connectivity resemble those of other mGCs [45,46]. Prior to this, during a critical period of their development when neurons are between 4-8 weeks post mitosis, it has been proposed that the cellular properties and connectivity in the microcircuit imbue unique roles for abDGCs, functionally distinguishing them from mGCs [47], including involvement in behaviors that require discrimination of similar contexts [48,49]. Notably, it has been proposed that abDGCs affect the local circuit by contributing to the sparsity of mGC activity through feedback inhibition [47,50,51] or through direct inhibition [52]. This inhibitory influence is largely mediated by diverse interneuron populations in the DG, including parvalbumin-positive (PV+), somatostatin-positive (SOM+), and neuropeptide Y-positive (NPY+) interneurons, which play crucial roles in regulating the excitability of GCs. Given their importance in enforcing sparse coding, these interneurons could be key modulators of the SB-IB activity differences observed in our study, yet their precise contribution to blade-specific activation remains unclear. Investigating their role will be critical in understanding how inhibitory networks shape the DG's computational function. Transformations of cortical inputs to sparse representations in the DG are a prerequisite for the distributed code required to separate similar input patterns. Behavioral experiments support the involvement of the DG in pattern separation [53]. Manipulations that ablate abDGCs cause impairments in spatial discrimination when the task is made more challenging with less separation between the locations [54]. Conversely genetic or environmental manipulations aimed at increasing neurogenesis enhance the ability of animals in spatial discrimination tasks [48,55]. In our experiments we detected limited numbers of labeled abDGCs during performance of a task as might be expected given that the population of these neurons is much lower that mGCs. However, we did observe that older neurons that were ~7 weeks post mitosis were more prominently labeled compared to ~4 week postmitotic neurons as might also be expected given these are more connected to the local network. Importantly these neurons had an outsized influence on the DG. We used an acute and reversible method to chemogenetically inhibit different cohorts of abDGCs just during task performance [36], and similar to studies which have made chronic manipulations of neurogenesis [31] found that there was a general increase in active mGCs. More importantly acute inhibition of abDGCs during the LS task reduced performance of mice in the high cognitive demand discrimination trials without degrading their performance in already established low demand discrimination trials in the same

sessions. Analysis of active labeled mGCs in mice that successfully navigated the task but with reduced performance demonstrated a correlated effect on the spatial distribution of labeled neurons in the DG. The enhanced SB to IB biased activity of mGCs was not observed. In addition, the characteristic distribution of mGCs along the hilar to molecular layer axis of the DG and from the dentate apex to the blade tips when mice performed the high cognitive demand task was also not observed when the abDGCs were chemogenetically inhibited. Again, these effects were only observed when cohorts of $\leq$ 7-week-old abDGCs were targeted with the DREADD but not when cohorts of $\leq$ 4-week-old abDGCs were inhibited. Therefore, our results reveal an important role for abDGCs in affecting dentate activity patterns and behaviors that impose a higher cognitive demand likely through this modulatory effect on the DG rather than serving as direct encoders of information [56]. This is consistent with a model where the required activity representation in the dentate for efficient pattern separation is influenced by cohorts of abDGCs as they are maturing through their critical period by both sparsening and influencing the spatial distribution of active mGCs.

Activity levels of mGCs is required for a high demand task

In our final experiment we used an acute and reversible DREADD inhibition of mGCs using a Cre driver line expressed in mGCs but not in young abDGCs neurons (Figure 6A, S3). mGCs are sparsely active in vivo [57] which is a key feature of dentate circuit function. However, imposing a chemogenetic suppression of their activity during the LS task had a major effect on the performance of mice with a majority of the tested cohort not reaching criterion. Analysis of these mice demonstrated that during S trials they remained at chance whereas they continued to perform above criterion at interleaved L trials (not shown). Consistent with inhibition of mGCs activity, c-Fos+ neuron density was reduced in the DG, however surprisingly the blade biased distribution of active neurons was evident in mice that performed the task but were not successful in reaching criterion. Thus, unlike with abDGC inhibition experiments there was not a clear correlation between effects on behavior in the LS task and the spatial distribution of active cells. This demonstrates that the effect of direct inhibition of mGCs produces a fundamentally different result on the activity of the circuit that affects the behaviors accordingly. While for abDGC DREADD inhibition slowed performance in the successful completion of the task, even in mice that reached criterion there was altered spatial distribution of active mGCs. In the case of direct inhibition of mGCs overall excitability was altered but the spatial pattern of activity was not in mice that did or did not reach criterion (not shown). Moreover, the subset of mice that did reach criterion did so in a time indistinguishable from the control cohort (not shown). Prior studies using genetic manipulations to increase neurogenesis, have identified blade-specific

changes in the number of c-Fos+ cells, with an increase in the IB following contextual discrimination [58], and a corresponding increase or decrease in the IB or SB respectively, after navigational learning [59]. These findings support the hypothesis that the SB is context-specific and involved in pattern separation, while the IB is more associated with spatial representation and memory precision, a notion further corroborated by our study [56].
Overall, our results demonstrate an amplification in SB-IB activity bias of mGCs during the performance of a high cognitive demand task. Future studies will be required to fully understand the functional significance of this patterned distribution and whether this spatial bias actively contributes to enhanced pattern separation or merely reflects inherent blade-specific properties of the DG.

Limitations of the Study

The use of activity tagging has the inherent limitation that it provides a snapshot in time of activity during a window and more nuanced effects of activity patterns during the behaviors are not captured. This is countered by the less invasive nature of these experiments than ones that require implants for in vivo recording of neuron activity, which are themselves not fit for purpose because they cannot capture the spatial distribution in the subregions of the DG effectively. Future studies using *in vivo* measurements of activity will be required to support the present findings and find conclusive neural representations required for discrimination of similar patterns. A second limitation is that the mechanisms of the blade biased activity are yet to be discovered. Future work will be needed to assess this to further elucidate the importance of these patterns of activity to computations in the DG.

Materials and methods

Ethics statement: All animal procedures were conducted in accordance with protocols approved by the Northwestern University Institutional Animal Care and Use Committee (IACUC). Male and female mice were housed 3–5 per cage on a reverse light/dark cycle of 12/12 hours within a controlled environment. They received food and water *ad libitum*. All behavioral testing was conducted during the animals' dark cycle and was conducted by experimenters blinded to genotype. Tail biopsies were collected for genotyping via PCR. All efforts were made to minimize the number of mice used and to reduce any potential pain or stress, in line with ethical guideline.

Animals: All mouse lines were maintained on a C57Bl/6 background. Mice were propagated by female breeders heterozygous for Cre recombinase and homozygous for either the Ai9 allele (Rosa-CAG-LSL-tdTomato-WPRE) or hM4Di allele (R26-LSL-Gi-DREADD) with male breeders

homozygous for Ai9 or hM4Di. TRAP2;Ai9 mice were generated by crossing Fos$^{2A-iCreER/+}$ (TRAP2) mice (Jax #030323)[23] with Ai9 (Jax #007909) mice to generate double-heterozygous mice. Ascl1-CreER^{T2};hM4Di mice were generated by crossing R26-LSL-Gi-DREADD mice (Jax #026219) [33] with mice carrying tamoxifen-inducible Cre recombinase under the control of the *Ascl1* promoter (Jax #:012882) [60] to generate double-transgenic progeny Ascl1-CreER^{T2};R26$^{LSL-hM4Di}$. Cre-negative littermates from heterozygote breedings were used as controls. Dock10-Cre;hM4Di mice were generated by crossing Dock10-Cre [42] mice with hM4Di mice to produce double-transgenic progeny Dock10-Cre;R26$^{LSL-hM4Di}$.

Birth-dating of abDGCs: 6–8-week-old mice received three intraperitoneal (i.p.) injections of 5-Bromo-2′-deoxyuridine (BrdU, Sigma Aldrich #B9285) at 100 mg/kg (i.p) at 4 hours intervals on a single day [61]. Two weeks later, 5-Ethynyl-2′-deoxyuridine (EdU, Sigma Aldrich, #900584) was administrated following the same injection protocol.

Tamoxifen administration: *IP injections:* To time the labeling of TRAP+ cell in TRAP2 mice, 4-hydroxytamoxifen (4-OHT; Sigma Aldrich, #H7904) was administered intraperitoneally. 4-OHT was dissolved at 20 mg/mL in pure ethanol and stored at –20°C for up to several weeks. Before use, 4-OHT was redissolved in corn oil (Sigma, Cat #C8267) and heated to 90°C with shaking until the ethanol had evaporated yielding a final concentration of 10 mg/mL. The final 10 mg/mL 4-OHT solutions was used on the day it was prepared. All injections were delivered intraperitoneally at 50 mg/kg either at the end of the training phase of the day or 2 hours after running.
Oral administration: For conditional expression of hM4Di in *Ascl1-CreER^{T2}* cells, a tamoxifen diet (TD.130858, Envigo) was provided *ad libitum* for 4 or 7 weeks, depending on the experimental timeline. Body weight was carefully monitored daily. The chow contained 500 mg tamoxifen/kg, delivering ~80 mg tamoxifen/kg body weight per day, assuming an average mouse weight of 20-25 g and a daily intake of 3-4 g.

Inhibitory DREADD-hM4Di activation: Deschloroclozapine (DCZ, MedChemExpress #HY-42110) was dissolved in 2% DMSO in 0.9% saline and administered by i.p. injections at a dose of 50 μg.kg^{-1} [34]. Behavioral trials started 30 minutes after drug administration.
Behavioral procedures: Adult (8-10 weeks-old) male and female mice were used in behavioral studies. To acclimate the mice to handling before behavioral testing, all animals were handled by the experimenter for 2 min per day for 3 consecutive days.

Running wheels: To habituate the mice to running, wireless running wheels (ENV-047, Med Associates) were placed in their home cage for 5 days (maximum 5 mice per cage). Two days

prior to BrdU injections, the wheels were removed from the cage. One week before the experiment, mice were individually housed. On the day of the experiment, a running wheel was added to each cage for a duration of 4 hours. After 2 hours, mice received a 4-OHT injection and were returned to their respective cages. Following an additional 2 hours of running, the wheels were removed from the cages. Three days later, wheels were reintroduced to the cage and remained until mice were euthanized for assessment of TRAP+ cells, 90 minutes after the beginning of the run. The effect of exposure to the wheels was quantified by measuring the total distance run by each mouse.

Automated touch screen operant behaviors: Testing was conducted in custom-built, touch screen-based automated operant device boxes designed specifically for mice, the Operant House (doi.org/10.1101/2025.01.24.634815). The apparatus consisted of a rectangular modular testing chamber (w14.5cm x l21.5cm x h18.5cm). A 60mW green LED was located above a port that gave access to a retractable water bottle at the back of the chamber. At the opposite end of the chamber, a flat-screen infrared touch monitor was controlled by custom scripts (Python). In front of the touchscreen was a mask with 2 horizontal lines of 5 squares. Mice performed a modified version of the “trial unique nonmatching-to-location” (TUNL) task [29]. Five days prior to testing and during the training phase, mice were placed on a water-restriction regime, with access to water for 10 minutes per day, and were maintained at 85-90% body weight during the entire duration of the experiment. Mice were trained each day, in two separate sessions of 30 trials or a maximum of 30 minutes. Experiments began with “Shaping” in which, following habituation to the operant chamber for 30 minutes, mice were trained to touch a lit white square stimulus presented randomly in one of the response windows of the touch screen in order to receive a reward (2 seconds water nozzle access with saccharin water 0.01%). Mice were trained in Shaping until they successfully achieved 30 rewards within 30 min during 3 successive sessions. Mice were then transitioned to training in the TUNL task with a Large-only separation (L configuration). For this task, each trial was composed of two phases. During the sample phase, a white square was illuminated in one of the 10 possible locations on the screen (Figure S2A & B). Following a nose-poke to the sample square the stimulus disappeared, and the mouse received a reward only on 33% of the trials. After a 1s delay from the sample trial, the choice trial was initiated where two stimuli were presented one in the repeated sample location (incorrect) and the other in the new location (correct) separated spatially by 4 squares in the L configuration (Figure S2A & B). A touch to the correct sample location resulted in a reward and an 5s inter-trial interval (ITI) before the next trial was initiated. An incorrect choice resulted in a 10 second punishment (roof lights ON) and then an ITI, followed by correction trials

during the first two days of training. Correction trials followed the same procedures, except that the same sample and choice locations from the previous incorrect trial were presented again until the correct choice was made. The correction trials were not included in performance calculations. After successfully completing 30 trials within 30 minutes at over 70 % correct for at least two out of four sessions on two consecutive days in the Large configuration, the mice were transitioned to the next phase of the TUNL task with combined sessions with presentation of stimuli with both Large separation and Small separation between sample and choice squares (LS configuration). Training followed the same pattern as previously described except that there were two separate possibilities for the presentation of the choice square which was either separated by 4 squares from the sample square during L trials, or the choice square was 0-1 square separated from the sample location during S trials (Figure S2B). Mice trained in the LS phase with 15 of each alternating L and S trials, until they reached criterion which was set at 70 % successful S configuration trials in two out of four sessions on two days. A proportion of mice did not reach the criterion in LS within the allotted time across all experimental groups (~25%-30%, Figures S2F).

Immunohistochemistry: Mice were deeply anesthetized with isoflurane and then perfused transcardiacly with PBS containing 0.02% sodium nitrite followed by 2% paraformaldehyde (PFA) in 0.1 M sodium acetate buffer (pH 6.5) for 3 min, and 2% PFA in 0.1 M sodium borate buffer (pH 8.5) for 10 min [62]. Brains were dissected and post-fixed in 2% PFA 0.1 M sodium borate buffer (pH 8.5), for 24-48 hours and stored at 4°C in PBS until sectioning. 50µm floating sections were collected on a Leica Vibratome VT1000 and stored at 4°C in PBS containing 0.02% sodium azide. For c-Fos analysis, perfusions were performed 90 minutes after the end of the behavioral training. Immunohistochemistry was conducted at room temperature using standard procedures. Free-floating sections were incubated for 30 min in a solution of 25 mM glycine to decrease the background signal and then rinsed two times in Tris-Buffered Saline 1X (TBS). Sections were then blocked for 1 hour in the saturation solution containing TBS-Triton (0.25% Triton X-100 (Fisher, BP151-100), 3% normal donkey serum (NDS; Jackson ImmunoResearch, 017-000-121) and 0.1% bovine serum albumin (BSA; Sigma, A9085)). The sections were then incubated overnight in the saturation solution containing the primary antibody (rabbit anti c-Fos (1/1500, Cell Signaling), sheep anti-BrdU (1/2500, NovusBio), rabbit anti RFP (1/5000, Abcam)). For c-Fos staining, no serum and BSA were used. For BrdU staining, sections were incubated for 10 mins in a solution of DNAse I (Sigma #D5025, 15 KU/mL dissolved in 0.05 M NaCl), $MgCl^2$ (6 mM) and $CaCl^2$ (10 mM) to cleave DNA then rinsed 2 x 5 min in TBS before the saturation part. For EdU staining, sections were incubated in

solution from the kit ClickIT™ (#C10340 Thermofisher) during 30 min then rinsed 2 x 5 min TBS before the saturation part. No antibodies were necessary for the rest of the immunostaining. The next day, sections were washed 2x5 min in TBS before being incubated for 1 hour in secondary antibody solution (donkey anti-rabbit Alexa 647 or 488 (1/1000, Invitrogen), donkey anti-sheep Alexa 488 (1/1000, Invitrogen)). Finally, sections were washed 2x5 min in TBS and cover-slipped with ProLong Diamond mounting media 275 containing DAPI (#P36962, ThermoFisher Scientific).

Imaging and neuron quantification: Analyses were conducted in the dorsal DG, as prior studies have demonstrated its involvement in spatial memory and the fine-grained contextual differentiation required for pattern separation. The dorsal hippocampus is crucial for encoding and distinguishing spatial information, which is central to this process. In contrast, the ventral DG is more strongly associated with emotional processing and affective memory rather than high-resolution spatial encoding needed for pattern separation.

Confocal images were obtained with a Zeiss microscope (LSM700) with a 20x objective with the experimenter blind to the genotype and condition following previous protocols [61]. One section in every ten serial sections were analyzed through the dorsal hippocampus (stereotaxic coordinates: -1.20 to -2.30 relative to bregma according to Paxinos' brain atlas). Two to three 10 µm z-stack acquisitions, were made to picture the whole dentate gyrus in each section. 3D reconstructions were used to univocally verify co-localization (e.g. activated mature neurons or immature neurons). All acquisitions were carried out in sequential scanning mode to prevent cross-bleeding between channels. Stacks of images were then reconstituted using Fiji software, allowing the experimenter to count the number of cells. The surface area of the dorsal hippocampus, DG, SB, IB and CA3 were traced in mapping software (Neurolucida Zeiss) using a 10x objective. The volume was determined by multiplying the surface area by the distance between sections (500 µm). Densities of BrdU+, EdU+, TRAP+ and c-Fos+ cells were estimated by multiplying the total number of labeled cells by 10. For immunohistochemical analysis, a subset of approximately 5 mice from the behavioral cohorts of ~15 mice were randomly selected. If the results exhibited high variability, one or two additional mice were included to improve data precision. Selection remained random throughout. This approach was chosen to balance the workload associated with immunohistochemistry while ensuring sufficient statistical power; given that behavioral experiments require larger sample sizes to achieve robust significance only a subset could be included in this analysis.

Distribution of TRAP+ and c-Fos+ Cells in the DG: We followed methods presented in literature [63]. Using stacks of images obtained from confocal microscopy, the localization of TRAP+ and c-Fos+ cells in the DG was assessed using Fiji software. *Distance from the hilus:* The contours of each blade were manually outlined and the distance from the center of each cell body to the hilus was manually measured. Cells located in the apex region were excluded from the counting.

Distance from the apex: Excluding the apex region, the size of each suprapyramidal blade was measured as well as the distance of each cell from the apex. These distances were then expressed as percentage of total blade length.

Statistical analysis: Data are expressed as means ± SEM. Statistical analysis was performed using Statview and Origin programs. For behavioral experiments, one sample *t*-tests were used to compare performance against chance (50% in the TUNL experiment). For histochemical data, we used independent comparisons with Mann–Whitney U test for non-paired samples (non-parametric). To test more than two independent samples we used the Kruskal Wallis test. In case of significance, a post hoc pairwise comparison (Dunn's test) was made to identify the group that differed. Differences were considered to be significant when $p < 0.05$.

Figure Legends:

Figure 1 : **TRAP labeling of mGCs and birth-dated abDGCs after the TUNL pattern separation task**

(A) *Top:* Schematic illustrating the pattern separation paradigm. Male (n = 9) and female (n = 7) mice (6-8-week-old) received 3 injections of BrdU at D0 and 3 injections of EdU two weeks later (D14) before starting the behavioral paradigm. Mice received one injection of 4-OHT on the day they reached criterion (TRAP) and were perfused 3 days later 90 minutes after one exposure to the behavioral paradigm to allow endogenous c-Fos expression (c-Fos). Control mice (males n = 6, females n = 4) underwent the same treatment but only participated in the Large separation task (L). Mice were water-restricted during the behavioral experiment. *Bottom:* Cartoon representation of the chamber in TUNL task with examples of Large separation (L) and Small (S) separation configurations. High cognitive demand paradigm consisted of interleaved L and S trials (LS).

(B) Number of days for each mouse to reach the 70% success criterion in the Large separation (L).

(C) Number of days for mice to reach 70% success criterion in S trials, during the LS separation task.

(D) *Left*: Average percentage of correct choices (% success) in the L separation on the first day of training, as well as during the three days prior to reaching criterion (days before criterion, DBC) and the day of reaching the criterion (crit)(one-sample *t*-test to chance at criterion Large $t(16)=12.04$, $p<0.0001$). *Middle*: Average percentage of correct choices in the L and S separation on the first day of training, during the three days before criterion (DBC), on the day of reaching criterion and 3 days later (one-sample *t*-test to chance at criterion Large $t(16)=8.38$, $p<0.0001$; Small $t(16)=7.37$, $p<0.0001$). *Right:* Cumulative probability of days to criterion of mice in S for both controls L and LS groups.

(E) Example section of BrdU+ labeling (green) EdU+ labeling (blue) and TRAP+ labeling (red) in TRAP2 mice. Calibration bar: 30 µm.

(F) Density of TRAP-labeled GCs in mice undergoing LS compared to control mice engaged in either shaping (Shap) or the Large configuration task only (L) ($H(2) = 7.42$, $p =0.0245$; Kruskal Wallis)(With Dunn post hoc analysis: Shape comparison to L, $p = 0.112$, Shape comparison to LS, $p=0.007$, L comparison to LS $p = 0.194$).

(G) Percentage of BrdU labeled cells (39 days +/- 1.23) or Edu labeled cells (25 days +/- 1.37 days) also TRAP+ after L or LS training (BrdU+/TRAP+ L: 0.145 ± 0.145 %, 6 mice; LS BrdU+/TRAP+ 0.822 ± 0.474 %, 6 mice; ns; EdU+/TRAP+ L: 0.203 ± 0.144 %, 6 mice; LS BrdU+/TRAP+ 0.304 ± 0.155 %, 7 mice; ns; Mann–Whitney).

(H) Percentage of TRAP+ GCs expressing c-Fos+ in the L or LS task after reaching criterion (expressed as a percentage of TRAP+ cells) (L TRAP+/c-Fos+: 1.578 ± 1.119 %, 4 mice; LS TRAP+/c-Fos+: 3.926 ± 2.277 %, 6 mice; $p = 0.05$; Mann–Whitney).

Figure 2: **Blade-biased activity of mGCs during a high cognitive demand pattern separation task**

(A) Spatial distribution of TRAP-labeled cells in the infrapyramidal (IB) and suprapyramidal (SB) blades of the dorsal DG in TRAP2 mice performing the LS separation, compared to control mice that performed only the L configuration. TRAP+ neurons showed a preferential distribution to the SB over the IB in the DG, with a more pronounced bias in the LS group of mice (IB : L: 43.410 ± 1.51 %, 6 mice; LS : 34.01 ± 2.79 %, 8 mice; p= 0.0282; SB : L: 56.56 ± 1.51 %, 6 mice; LS : 65.99 ± 2.79 %, 8 mice; p= 0.0282; Mann–Whitney)

(B) Spatial distribution of TRAP+ cells in the hilar to outer radial GCL axes in the SB (0 to 120µm) and the IB (0 to 120µm) of the dorsal DG with 0 µm indicating location at the hilar border.

(C) Distribution of TRAP-labeled cells along the apex to blade extremity axes of the SB of the dorsal DG, with 0% indicating location at the dentate apex (L: 0-50: 51.9 ± 2.18 %, 6 mice; 50-100: 48.1 ± 2.18 %, 6 mice; ns ; LS : 0-50: 56.0 ± 2.44 %, 6 mice; 50-100: 43.8 ± 2.54 %, 6 mice; p= 0.0065; Mann–Whitney).
(D) Example section of TRAP+ cells in the dorsal DG illustrating the distinct boundaries between the two blades, the hilus, and the apex. Calibration bar: 50 µm.
(E) Cartoon illustrating the two blades of the DG: IB and SB. Dentate granule cells are depicted in grey while red circles represent TRAP+ cells in the DG. In the L group, a greater number of labeled cells are localized in the SB compared to the IB. This bias of activity is also observed in the LS group, where the bias is more pronounced, and the overall activity of the DG is increased. In the SB, the majority of the activated cells are located closer to the apex region.

Figure 3: **Activation of GCs during remote recall in the high cognitive demand task**
(A) Schematic representation of the pattern separation paradigm used in the study. Mice (male n=11, female n=8) performed two trainings sessions: initial (I) and remote (R). The second training (R) took place 3 weeks after the mice reached the S criterion in LS. Mice were perfused when they reached the criterion in S during R. A second group that performed only in the L configuration during both training sessions was included as control (males n=3, females n=3).
(B) Learning curves representing the percentage of success during the remote test (R) for the L (green) and LS (orange) groups (one-sample *t*-test to chance at criterion; LS: Large $t(14) = 11.8$, $p < 0.0001$, Small $t(14) = 10.3$, $p<0.0001$; L: Large $t(3) = 6.78$, $p = 0.0066$).
(C) Percentage of mice reaching the L and S criterion in LS group, during the remote test (R) represented as cumulative probability. During the remote test, mice reach the L criterion in just a few days but require more time to reach the S criterion.
(D) Performance of individual mice indicating a non-significant reduction in the number of days needed to reach the criterion between the initial and remote training sessions. Only 4 mice (red lines) required more days to reach the criterion during the remote test. (I: 8.067 ± 1.173 %, R: 5.93 ± 0.753, 15 mice; p= 0.204; Mann–Whitney).
(E) EdU labeled cell that was also TRAP+ labeled after the initial training but was that was not reactivated (c-Fos) during the remote test. EdU (green), TRAP (red), c-Fos (blue) in TRAP2 mice. Calibration bar, 10 µm.
(F) Distribution of TRAP-labeled cells in the IB and SB blades of the dorsal DG in TRAP2 mice. Labeling was performed in LS separation during initial training (I) and compared to control mice that performed only the L configuration. Active neurons show a preferential distribution to the SB

over the IB in the DG. This bias is more prominent in the LS group of mice (training I: IB : L: 47.3 ± 3.312 %, 4 mice; LS : 33.7 ± 3.31 %, 4 mice; p = 0.021; SB : L: 52.7 ± 3.32 %, 4 mice; LS : 66.4 ± 3.31 %, 4 mice; p= 0.021; Mann–Whitney).

(G) Distribution of c-Fos labeled cells between the IB and SB blades of the dorsal DG in TRAP2 mice performing the LS separation during remote training (R), compared to control mice that performed only the L configuration. Active neurons show a preferential distribution to the SB over the IB in the DG (LS, IB : 31.4 ± 3.11 %, 4 mice; SB : 68.7 ± 3.11 %; p=0.021; Mann–Whitney). The bias of activity is similar between the two groups (R, IB : L: 41.1 ± 4.18 %, 4 mice; LS : 31.4 ± 3.101 %, 4 mice; p= 0.191; SB : L: 58.9 ± 4.18 %, 4 mice; LS : 68.7 ± 3.11 %, 4 mice; p= 0.191; Mann–Whitney).

(H) Percentage of newborn neurons (BrdU (7.7 weeks) or EdU (5.7 weeks)) activated during the initial training (I), as indicated by co-labeling of $TRAP^+$(BrdU+ c-Fos+: L: 0.242 ± 0.242 %, 6 mice, LS: 0.170 ± 0.170 %, 6 mice; ns ; Mann–Whitney).

(I) Percentage of newborn neurons (BrdU or EdU) activated during the remote test (R), as indicated by c-Fos expression (BrdU+ c-Fos+: 0.977 ± 0.426 %, 6 mice, p=0.05; EdU+ c-Fos+: 0.694± 0.317 %, 9 mice; p= 0.0785; Mann–Whitney).

(J) Percentage of mGCs activated during the (I) training ($TRAP^+$) that were reactivated during the R test (c-Fos+) (expressed as a percentage of TRAP+ cells) (TRAP+ c-Fos+: I: 0.764 ± 0.309 %, 4 mice; R: 1.68 ± 0.067 %, 4 mice; p= 0.0433; Mann–Whitney).

Figure 4: **DREADD inhibition of ≤ 7-week abDGCs during a high cognitive demand task**

(A) Schematic representation of the pattern separation paradigm. Prior to onset of the training, mice (males n = 17, females n = 16) were provided tamoxifen-containing food ad libitum in the home cage for 7 weeks to activate TAM inducible Cre recombinase (Ascl1-$CreER^{T2}$) in abDGCs. All mice received DCZ (deschloroclozapine, 50 $\mu g.kg^{-1}$) or DMSO injections 30 minutes before the beginning of LS trials.

(B) Example section from Ascl1-$CreER^{T2}$; hM4Di mice after LS training. c-Fos+ neurons are labeled in red, TAM induced neurons expressing citrine are labeled green. Calibration bars *top*: 140 µm *bottom*: 50 µm.

(C) Percentage of mice reaching the criterion in the S trials across days represented as the cumulative probability. The Cre+ DCZ treated group needed additional days to reach criterion compared to controls.

(D) Number of days for each mouse to reach the 70% success criterion in S trials, ($H(2) = 6.29$, $p=0.043$; Kruskal Wallis)(Cre+ DCZ comparison to Cre+ DMSO, $p = 0.017$; Cre+ DCZ comparison to Cre- DCZ, $p = 0.05$ with Dunn's multiple comparison post hoc analysis).
(E) c-Fos+ cell density in all groups of mice. There was an increase in c-Fos+ mGCs in mice in which ≤ 7 week abDGCs were inhibited by DCZ ($H(2) = 7.22$, $p=0.0271$; Kruskal Wallis)(Cre+ DCZ comparison to Cre+ DMSO, $p = 0.014$; Cre+ DCZ comparison to Cre- DCZ, $p = 0.027$ with Dunn's multiple comparison post hoc analysis).
(F) Example section after c-Fos immunohistochemistry to assess distribution of c-Fos+ mGCs between the IB and SB of the dorsal DG in groups of mice who received DCZ (cre- vs cre+). c-Fos cells are localized closer to the hilus in the Cre+ group. Calibration bar, 100 μm.
(G) c-Fos+ density in the CA3 region of the hippocampus in each of the groups of mice. No significant difference was observed in any of the groups ($H(2) = 3.9$, $p =0.142$; Kruskal Wallis).
(H) Blade distribution of c-Fos+ mGCs in the IB and SB of the dorsal DG in mice performing the LS separation receiving either DCZ or DMSO 30 min prior to task performance. Active neurons are distributed preferentially to the SB than the IB in the DG for the control groups. However this distribution bias is significantly reduced in Cre+ DCZ group (IB: $H(2) = 8.91$, $p = 0.012$; SB: $H(2) = 8.910$, $p = 0.012$; Kruskal Wallis)(Cre+ DCZ comparison to Cre- DCZ $p = 0.0032$; Cre+ DCZ comparison to Cre+ DMSO $p = 0.036$ with Dunn's multiple comparison post hoc analysis).
(I) Spatial distribution of c-Fos+ GCs along hilar to molecular layer axes of the SB (0 to 120μm) and the IB (0 to 120μm) of the dorsal DG, with 0 μm indicating the hilar position. c-Fos+ cells are localized closer to the hilus in the Cre+ DCZ group.
(J) Cartoon illustrating the DG with its two blades: IB and SB. Dentate granule cells are depicted in grey while red circles represent activity labeled cells in the DG. For Cre+ DCZ mice, the distribution of labeled neurons is closer to hilus, away from outer radial GCL and more evenly distributed in IB and SB.

Figure 5: **DREADD inhibition of ≤ 4-week-old abDGCs does not affect performance of mice**
(A) Schematic representation of the pattern separation paradigm used in the study. Prior to the behavioral experiment, mice (males n = 12, females n = 23) were given tamoxifen-enriched food for 4 weeks to activate the Cre recombinase and label newborn neurons. All mice received DCZ or DMSO injections 30 minutes before the beginning of LS trials.
(B) Number of days for each mouse to reach the 70% success criterion in S trials ($H(2) = 4.21$, ns; Kruskal Wallis).

(C) Density of c-Fos+ GCs in the dorsal DG across the different groups (DG: H(2) = 0.404, ns, Kruskal Wallis)
(D) Blade specific distribution of c-Fos+ cells in the IB and SB of the dorsal DG in mice performing LS separation (H(2) = 0.46, ns ; Kruskal Wallis).
(E) Spatial distribution of c-Fos+ along the hilar to outer radial GCL axis of the DG (0 to 120µm), with 0 µm indicating location at the hilus.

Figure 6: **DREADD inhibition of mGCs during a high cognitive demand task**
(A) Percentage of BrdU-labeled cells that are also Dock10+ at different time points following BrdU injections (in days).
(B) Representative section showing BrdU+ labeling (green) and Dock10+ labeling (red) in Dock10 cre;Ai9 mice. Calibration bars: 10 µm.
(C) Schematic representation of the pattern separation paradigm. All mice (males n = 17, females n = 27) received DCZ i.p. injections 30 minutes before the beginning of their LS trials.
(D) Percentage of mice reaching criterion in (S) and percentage that were not successful (NS) after 14 days of training in S configuration of LS. A majority of mice never succeeded in reaching the criterion in the Cre+ DCZ group (z = 2.00, p = 0.0453, z-test - Group NS).
(E) Percentage of mice reaching the criterion in S trials across days represented as the cumulative probability including all successful and not successful mice in the group.
(F) Density of c-Fos+ GCs in the dorsal DG across the two groups. A significantly reduced density was observed in the Cre+ DCZ group compared to controls (DG, Cre+ DCZ: 8933.9 ± 556.4 mm^3, 6 mice; Cre- DCZ: 13578 ± 2135 mm^3, 5 mice; p = 0.045; Mann–Whitney).
(G) Density of c-Fos+ GCs in the dorsal CA3 across the two groups. A significant reduction was observed in the Cre+ DCZ group compared to the control groups (CA3 Cre+ DCZ: 20647 ± 1309 mm^3, 6 mice; Cre-DCZ: 34500 ± 2665 mm^3, 5 mice; p= 0.0062; Mann–Whitney).
(H) Blade specific distribution of c-Fos+ GCs in the IB and SB of the dorsal DG in mice performing LS separation (IB: Cre- DCZ: 31.5 ± 2.47 %, 5 mice; Cre+ DCZ: 27.2 ± 2.55 %, 6 mice; ns; SB: Cre- DCZ: 68.6 ± 2.47 %, 5 mice; Cre+ DCZ: 72.8 ± 2.55 %, 6 mice; ns; Mann–Whitney).
(I) Example of dorsal DG section from Dock10-cre:hM4Di mice after LS training. c-Fos+ neurons are labeled in red, DREAD-hM4Di (=Dock10+) neurons expressing citrine are labeled in green. Calibration bars: 100 µm.
(J) Spatial distribution of c-Fos+ along the hilar to outer radial GCL axis of the DG (0 to 120µm), with 0 µm indicating location at the hilus.

(K) Cartoon illustrating the distribution of activity labeled GCs in the SB and IB blades of the DG. GCs are depicted in grey while red circles represent activated cells in the DG. The overall distribution of neurons in mice in which mGCs were inhibited (Cre+ DCZ) and which did not reach criterion was not different to controls even though the total density of activity labeled neurons was lower.

Figure Sup1: **Activity labeling of GCs after running**

(A) Schematic representation of the running paradigm. Prior to the behavioral experiment, mice (males n = 30, females n = 3) were injected with BrdU. After Δ weeks, the mice were allowed to run for 2 hours before receiving a 4-OHT injection, followed by an additional 2 hours of running. Mice were perfused 3 days later for immunohistochemistry of brain sections.

(B) Example section of immunohistochemistry of TRAP+ cells in the dorsal DG illustrating the distinct blades of the DG: SB and IB. Calibration bar: 40 µm.

(C) Density of TRAP+ GCs in mice after running compared to home cage controls (H). Each group represents mice that ran after variable time intervals following BrdU injections.

(D) Blade specific distribution of TRAP+ cells in the infrapyramidal (IB) and suprapyramidal (SB) blades of the dorsal DG in TRAP2 mice that ran for 4 hours, compared to home cage mice. (IB: home: 42.5 ± 1.43 %, 4 mice; run: 43.9 ± 1.42 %, 33 mice; ns; Mann–Whitney).

(E) Example section from mice labeled for BrdU (green), TRAP+ GCs (red) and endogenous c-Fos (blue) in TRAP2 mice. Calibration bar: 20 µm.

(F) Percentage of BrdU+ cells (Δ 1-14 weeks old) also labeled with TRAP in the dorsal DG of TRAP2 mice that ran for 4 hours, compared to home cage controls (H).

Figure Sup 2: **Description of the TUNL protocol and analysis of TRAP+ GCs in mice not meeting the criterion in the pattern separation task.**

(A) Overview of successive trials in the Shaping, L and LS steps. Mice must complete 30 trials at each step. The shaping phase involves touching the illuminated square to receive a reward. In the L and LS steps, there are in two phases: the sample (S) phase, where mice must touch the single illuminated square on the panel and the choice test (C), where two squares are illuminated: the previously touched square and a new one. Mice must nose poke the new square to receive the reward. In the L phase, trials consist only of L panels only (see Figure S2B – L). In the LS phase, L and S trials are alternated (see Figure S2B for S panels).

(B**)** Recommended stimulus pairs for the TUNL protocol. Large pairs (green) consist of 2 illuminated squares separated by 4 squares that are turned OFF. Small pairs (orange) consist of two illuminated squares separated by 0 to 1 square turned OFF.

(C) Correlation between the performance (= number of days to reach criterion) and the TRAP+ density or TRAP+ distribution in SB (D). Both regression analysis (right tables) show that the slope is not significantly different from zero.
(E) Comparison of TRAP+ distribution in IB and SB of the dorsal DG in mice from the home cage (Home), running (Run), large configuration (L) and large and small separation (LS) groups. In the control groups (Home, Run and L) the TRAP+ cells are predominantly distributed in the SB, with a slight preference for the SB over IB. However, in the high cognitive demand (CD), LS takm the distribution pf TRAP+ cells become more balanced, with a marked preference for the SB (SB >>IB), indicating task-specific modulation of activity across the blades.
(F) Percentage of TRAP2 mice reaching the criterion (C) compared to those that did not within 14 days of training (NC).
(G) Density of TRAP+ neurons in mice undergoing LS for mice that reached criterion (LS C) with mice that did not reach 70% criterion within 14 days (LS NC) (LS C: 2563 ± 481 mm^3, 8 mice; LS NC: 2036 ± 305 mm^3, 10 mice; ns; Mann–Whitney).
(H) Blade specific distribution of TRAP+ GCs in the SB and the IB of the dorsal DG (IB: LS C: 34 ± 2.79 %, 8 mice; LS NC : 33.8 ± 2.12 %, 12 mice; ns; Mann–Whitney).
(I) Percentage of TRAP+ cells also birth-dated with BrdU (39 days +/- 1.23) or Edu cells (25 days +/- 1.37 days) in the dorsal DG of TRAP2 mice that reached criterion (C) and those failed (NC)(BrdU: LS C: 0.71 ± 0.333 %, 7 mice; LS NC : 0.822 ± 0.45 %, 6 mice; ns; EdU: LS C: 0.542 ± 0.33 %, 9 mice; LS NC : 0.304 ± 0.16 %, 7 mice; ns; Mann–Whitney).

Figure Sup 3: **Dock10 is not expressed in -positive immature newborn neurons but is expressed in Prox1-positive neurons**
(A) Representative section from a Dock10-cre:Ai9 mouse following tdTomato (tdT), Prox1, and DCX immunohistochemistry in the dorsal DG. Calibration bar: 100 µm.
(B) 20X magnification of the suprapyramidal layer of the dentate gyrus, showing tdTomato (Dock10) in red, Prox1 in green, and DCX in blue. Calibration bar: 100 µm.
(C) tdT (Dock10) labeling. (D) Prox1 (green) labeling. (E) DCX (blue) labeling. Calibration bar: 100 µm.

Citations:

1. Hainmueller, T., and Bartos, M. (2020). Dentate gyrus circuits for encoding, retrieval and discrimination of episodic memories. Nat Rev Neurosci *21*, 153-168. 10.1038/s41583-019-0260-z.
2. Stefanini, F., Kushnir, L., Jimenez, J.C., Jennings, J.H., Woods, N.I., Stuber, G.D., Kheirbek, M.A., Hen, R., and Fusi, S. (2020). A Distributed Neural Code in the Dentate Gyrus and in CA1. Neuron *107*, 703-716 e704. 10.1016/j.neuron.2020.05.022.
3. Hunsaker, M.R., Rosenberg, J.S., and Kesner, R.P. (2008). The role of the dentate gyrus, CA3a,b, and CA3c for detecting spatial and environmental novelty. Hippocampus *18*, 1064-1073. 10.1002/hipo.20464.
4. Leutgeb, J.K., Leutgeb, S., Moser, M.B., and Moser, E.I. (2007). Pattern separation in the dentate gyrus and CA3 of the hippocampus. Science *315*, 961-966. 10.1126/science.1135801.
5. Altman, J., and Das, G.D. (1965). Autoradiographic and histological evidence of postnatal hippocampal neurogenesis in rats. J Comp Neurol *124*, 319-335. 10.1002/cne.901240303.
6. Kaplan, M.S., and Hinds, J.W. (1977). Neurogenesis in the adult rat: electron microscopic analysis of light radioautographs. Science *197*, 1092-1094. 10.1126/science.887941.
7. Cameron, H.A., Woolley, C.S., McEwen, B.S., and Gould, E. (1993). Differentiation of newly born neurons and glia in the dentate gyrus of the adult rat. Neuroscience *56*, 337-344. 10.1016/0306-4522(93)90335-d.
8. Kempermann, G., Kuhn, H.G., and Gage, F.H. (1997). More hippocampal neurons in adult mice living in an enriched environment. Nature *386*, 493-495. 10.1038/386493a0.
9. Folsz, O., Trouche, S., and Croset, V. (2023). Adult-born neurons add flexibility to hippocampal memories. Front Neurosci *17*, 1128623. 10.3389/fnins.2023.1128623.
10. Marr, D. (1969). A theory of cerebellar cortex. J Physiol *202*, 437-470. 10.1113/jphysiol.1969.sp008820.
11. Marr, D. (1971). Simple memory: a theory for archicortex. Philos Trans R Soc Lond B Biol Sci *262*, 23-81. 10.1098/rstb.1971.0078.
12. Rolls, E.T. (2016). Pattern separation, completion, and categorisation in the hippocampus and neocortex. Neurobiol Learn Mem *129*, 4-28. 10.1016/j.nlm.2015.07.008.

13. Borzello, M., Ramirez, S., Treves, A., Lee, I., Scharfman, H., Stark, C., Knierim, J.J., and Rangel, L.M. (2023). Assessments of dentate gyrus function: discoveries and debates. Nat Rev Neurosci *24*, 502-517. 10.1038/s41583-023-00710-z.
14. Amaral, D.G., Scharfman, H.E., and Lavenex, P. (2007). The dentate gyrus: fundamental neuroanatomical organization (dentate gyrus for dummies). Prog Brain Res *163*, 3-22. 10.1016/S0079-6123(07)63001-5.
15. Chawla, M.K., Guzowski, J.F., Ramirez-Amaya, V., Lipa, P., Hoffman, K.L., Marriott, L.K., Worley, P.F., McNaughton, B.L., and Barnes, C.A. (2005). Sparse, environmentally selective expression of Arc RNA in the upper blade of the rodent fascia dentata by brief spatial experience. Hippocampus *15*, 579-586. 10.1002/hipo.20091.
16. Scharfman, H.E., Sollas, A.L., Smith, K.L., Jackson, M.B., and Goodman, J.H. (2002). Structural and functional asymmetry in the normal and epileptic rat dentate gyrus. J Comp Neurol *454*, 424-439. 10.1002/cne.10449.
17. Erwin, S.R., Sun, W., Copeland, M., Lindo, S., Spruston, N., and Cembrowski, M.S. (2020). A Sparse, Spatially Biased Subtype of Mature Granule Cell Dominates Recruitment in Hippocampal-Associated Behaviors. Cell Rep *31*, 107551. 10.1016/j.celrep.2020.107551.
18. Snyder, J.S., Radik, R., Wojtowicz, J.M., and Cameron, H.A. (2009). Anatomical gradients of adult neurogenesis and activity: young neurons in the ventral dentate gyrus are activated by water maze training. Hippocampus *19*, 360-370. 10.1002/hipo.20525.
19. Dranovsky, A., Picchini, A.M., Moadel, T., Sisti, A.C., Yamada, A., Kimura, S., Leonardo, E.D., and Hen, R. (2011). Experience dictates stem cell fate in the adult hippocampus. Neuron *70*, 908-923. 10.1016/j.neuron.2011.05.022.
20. Jinno, S. (2011). Topographic differences in adult neurogenesis in the mouse hippocampus: a stereology-based study using endogenous markers. Hippocampus *21*, 467-480. 10.1002/hipo.20762.
21. Ramirez-Amaya, V., Marrone, D.F., Gage, F.H., Worley, P.F., and Barnes, C.A. (2006). Integration of new neurons into functional neural networks. J Neurosci *26*, 12237-12241. 10.1523/JNEUROSCI.2195-06.2006.
22. Alves, N.D., Patricio, P., Correia, J.S., Mateus-Pinheiro, A., Machado-Santos, A.R., Loureiro-Campos, E., Morais, M., Bessa, J.M., Sousa, N., and Pinto, L. (2018). Chronic stress targets adult neurogenesis preferentially in the suprapyramidal blade of the rat dorsal dentate gyrus. Brain Struct Funct *223*, 415-428. 10.1007/s00429-017-1490-3.

23. DeNardo, L.A., Liu, C.D., Allen, W.E., Adams, E.L., Friedmann, D., Fu, L., Guenthner, C.J., Tessier-Lavigne, M., and Luo, L. (2019). Temporal evolution of cortical ensembles promoting remote memory retrieval. Nat Neurosci *22*, 460-469. 10.1038/s41593-018-0318-7.
24. Castillon, C., Lunion, S., Desvignes, N., Hanauer, A., Laroche, S., and Poirier, R. (2018). Selective alteration of adult hippocampal neurogenesis and impaired spatial pattern separation performance in the RSK2-deficient mouse model of Coffin-Lowry syndrome. Neurobiol Dis *115*, 69-81. 10.1016/j.nbd.2018.04.007.
25. Chatzi, C., Zhang, Y., Hendricks, W.D., Chen, Y., Schnell, E., Goodman, R.H., and Westbrook, G.L. (2019). Exercise-induced enhancement of synaptic function triggered by the inverse BAR protein, Mtss1L. Elife *8*. 10.7554/eLife.45920.
26. Deng, W., Mayford, M., and Gage, F.H. (2013). Selection of distinct populations of dentate granule cells in response to inputs as a mechanism for pattern separation in mice. Elife *2*, e00312. 10.7554/eLife.00312.
27. Lamothe-Molina, P.J., Franzelin, A., Beck, L., Li, D., Auksutat, L., Fieblinger, T., Laprell, L., Alhbeck, J., Gee, C.E., Kneussel, M., et al. (2022). DeltaFosB accumulation in hippocampal granule cells drives cFos pattern separation during spatial learning. Nat Commun *13*, 6376. 10.1038/s41467-022-33947-w.
28. Talpos, J.C., McTighe, S.M., Dias, R., Saksida, L.M., and Bussey, T.J. (2010). Trial-unique, delayed nonmatching-to-location (TUNL): a novel, highly hippocampus-dependent automated touchscreen test of location memory and pattern separation. Neurobiol Learn Mem *94*, 341-352. 10.1016/j.nlm.2010.07.006.
29. Oomen, C.A., Hvoslef-Eide, M., Heath, C.J., Mar, A.C., Horner, A.E., Bussey, T.J., and Saksida, L.M. (2013). The touchscreen operant platform for testing working memory and pattern separation in rats and mice. Nat Protoc *8*, 2006-2021. 10.1038/nprot.2013.124.
30. Williams, P.A., Larimer, P., Gao, Y., and Strowbridge, B.W. (2007). Semilunar granule cells: glutamatergic neurons in the rat dentate gyrus with axon collaterals in the inner molecular layer. J Neurosci *27*, 13756-13761. 10.1523/JNEUROSCI.4053-07.2007.
31. Ikrar, T., Guo, N., He, K., Besnard, A., Levinson, S., Hill, A., Lee, H.K., Hen, R., Xu, X., and Sahay, A. (2013). Adult neurogenesis modifies excitability of the dentate gyrus. Front Neural Circuits *7*, 204. 10.3389/fncir.2013.00204.
32. Drew, L.J., Kheirbek, M.A., Luna, V.M., Denny, C.A., Cloidt, M.A., Wu, M.V., Jain, S., Scharfman, H.E., and Hen, R. (2016). Activation of local inhibitory circuits in the dentate gyrus by adult-born neurons. Hippocampus *26*, 763-778. 10.1002/hipo.22557.

33. Zhu, H., Aryal, D.K., Olsen, R.H., Urban, D.J., Swearingen, A., Forbes, S., Roth, B.L., and Hochgeschwender, U. (2016). Cre-dependent DREADD (Designer Receptors Exclusively Activated by Designer Drugs) mice. Genesis *54*, 439-446. 10.1002/dvg.22949.
34. Nagai, Y., Miyakawa, N., Takuwa, H., Hori, Y., Oyama, K., Ji, B., Takahashi, M., Huang, X.P., Slocum, S.T., DiBerto, J.F., et al. (2020). Deschloroclozapine, a potent and selective chemogenetic actuator enables rapid neuronal and behavioral modulations in mice and monkeys. Nat Neurosci *23*, 1157-1167. 10.1038/s41593-020-0661-3.
35. Yang, S.M., Alvarez, D.D., and Schinder, A.F. (2015). Reliable Genetic Labeling of Adult-Born Dentate Granule Cells Using Ascl1 CreERT2 and Glast CreERT2 Murine Lines. J Neurosci *35*, 15379-15390. 10.1523/JNEUROSCI.2345-15.2015.
36. Tunc-Ozcan, E., Peng, C.Y., Zhu, Y., Dunlop, S.R., Contractor, A., and Kessler, J.A. (2019). Activating newborn neurons suppresses depression and anxiety-like behaviors. Nat Commun *10*, 3768. 10.1038/s41467-019-11641-8.
37. Lacefield, C.O., Itskov, V., Reardon, T., Hen, R., and Gordon, J.A. (2012). Effects of adult-generated granule cells on coordinated network activity in the dentate gyrus. Hippocampus *22*, 106-116. 10.1002/hipo.20860.
38. Ge, S., Yang, C.H., Hsu, K.S., Ming, G.L., and Song, H. (2007). A critical period for enhanced synaptic plasticity in newly generated neurons of the adult brain. Neuron *54*, 559-566. 10.1016/j.neuron.2007.05.002.
39. Kennedy, W.M., Gonzalez, J.C., Lee, H., Wadiche, J.I., and Overstreet-Wadiche, L. (2024). T-Type Ca(2+) Channels Mediate a Critical Period of Plasticity in Adult-Born Granule Cells. J Neurosci *44*. 10.1523/JNEUROSCI.1503-23.2024.
40. Pilz, G.A., Carta, S., Stauble, A., Ayaz, A., Jessberger, S., and Helmchen, F. (2016). Functional Imaging of Dentate Granule Cells in the Adult Mouse Hippocampus. J Neurosci *36*, 7407-7414. 10.1523/JNEUROSCI.3065-15.2016.
41. Danielson, N.B., Kaifosh, P., Zaremba, J.D., Lovett-Barron, M., Tsai, J., Denny, C.A., Balough, E.M., Goldberg, A.R., Drew, L.J., Hen, R., et al. (2016). Distinct Contribution of Adult-Born Hippocampal Granule Cells to Context Encoding. Neuron *90*, 101-112. 10.1016/j.neuron.2016.02.019.
42. Kohara, K., Pignatelli, M., Rivest, A.J., Jung, H.Y., Kitamura, T., Suh, J., Frank, D., Kajikawa, K., Mise, N., Obata, Y., et al. (2014). Cell type-specific genetic and optogenetic tools reveal hippocampal CA2 circuits. Nat Neurosci *17*, 269-279. 10.1038/nn.3614.

43. Guzman, S.J., Schlogl, A., Espinoza, C., Zhang, X., Suter, B.A., and Jonas, P. (2021). How connectivity rules and synaptic properties shape the efficacy of pattern separation in the entorhinal cortex-dentate gyrus-CA3 network. Nat Comput Sci *1*, 830-842. 10.1038/s43588-021-00157-1.
44. van Praag, H., Schinder, A.F., Christie, B.R., Toni, N., Palmer, T.D., and Gage, F.H. (2002). Functional neurogenesis in the adult hippocampus. Nature *415*, 1030-1034. 10.1038/4151030a.
45. Zhao, C., Teng, E.M., Summers, R.G., Jr., Ming, G.L., and Gage, F.H. (2006). Distinct morphological stages of dentate granule neuron maturation in the adult mouse hippocampus. J Neurosci *26*, 3-11. 10.1523/JNEUROSCI.3648-05.2006.
46. Toni, N., Teng, E.M., Bushong, E.A., Aimone, J.B., Zhao, C., Consiglio, A., van Praag, H., Martone, M.E., Ellisman, M.H., and Gage, F.H. (2007). Synapse formation on neurons born in the adult hippocampus. Nat Neurosci *10*, 727-734. 10.1038/nn1908.
47. Temprana, S.G., Mongiat, L.A., Yang, S.M., Trinchero, M.F., Alvarez, D.D., Kropff, E., Giacomini, D., Beltramone, N., Lanuza, G.M., and Schinder, A.F. (2015). Delayed coupling to feedback inhibition during a critical period for the integration of adult-born granule cells. Neuron *85*, 116-130. 10.1016/j.neuron.2014.11.023.
48. Sahay, A., Scobie, K.N., Hill, A.S., O'Carroll, C.M., Kheirbek, M.A., Burghardt, N.S., Fenton, A.A., Dranovsky, A., and Hen, R. (2011). Increasing adult hippocampal neurogenesis is sufficient to improve pattern separation. Nature *472*, 466-470. 10.1038/nature09817.
49. Nakashiba, T., Cushman, J.D., Pelkey, K.A., Renaudineau, S., Buhl, D.L., McHugh, T.J., Rodriguez Barrera, V., Chittajallu, R., Iwamoto, K.S., McBain, C.J., et al. (2012). Young dentate granule cells mediate pattern separation, whereas old granule cells facilitate pattern completion. Cell *149*, 188-201. 10.1016/j.cell.2012.01.046.
50. Johnston, S.T., Shtrahman, M., Parylak, S., Goncalves, J.T., and Gage, F.H. (2016). Paradox of pattern separation and adult neurogenesis: A dual role for new neurons balancing memory resolution and robustness. Neurobiol Learn Mem *129*, 60-68. 10.1016/j.nlm.2015.10.013.
51. Dieni, C.V., Gonzalez, J.C., and Overstreet-Wadiche, L. (2019). Multifaceted circuit functions of adult-born neurons. F1000Res *8*. 10.12688/f1000research.20642.1.
52. Luna, V.M., Anacker, C., Burghardt, N.S., Khandaker, H., Andreu, V., Millette, A., Leary, P., Ravenelle, R., Jimenez, J.C., Mastrodonato, A., et al. (2019). Adult-born hippocampal

neurons bidirectionally modulate entorhinal inputs into the dentate gyrus. Science *364*, 578-583. 10.1126/science.aat8789.

53. Tuncdemir, S.N., Lacefield, C.O., and Hen, R. (2019). Contributions of adult neurogenesis to dentate gyrus network activity and computations. Behav Brain Res *374*, 112112. 10.1016/j.bbr.2019.112112.
54. Clelland, C.D., Choi, M., Romberg, C., Clemenson, G.D., Jr., Fragniere, A., Tyers, P., Jessberger, S., Saksida, L.M., Barker, R.A., Gage, F.H., and Bussey, T.J. (2009). A functional role for adult hippocampal neurogenesis in spatial pattern separation. Science *325*, 210-213. 10.1126/science.1173215.
55. Creer, D.J., Romberg, C., Saksida, L.M., van Praag, H., and Bussey, T.J. (2010). Running enhances spatial pattern separation in mice. Proc Natl Acad Sci U S A *107*, 2367-2372. 10.1073/pnas.0911725107.
56. Berdugo-Vega, G., Dhingra, S., and Calegari, F. (2023). Sharpening the blades of the dentate gyrus: how adult-born neurons differentially modulate diverse aspects of hippocampal learning and memory. EMBO J *42*, e113524. 10.15252/embj.2023113524.
57. Jung, M.W., and McNaughton, B.L. (1993). Spatial selectivity of unit activity in the hippocampal granular layer. Hippocampus *3*, 165-182. 10.1002/hipo.450030209.
58. Besnard, A., and Sahay, A. (2021). Enhancing adult neurogenesis promotes contextual fear memory discrimination and activation of hippocampal-dorsolateral septal circuits. Behav Brain Res *399*, 112917. 10.1016/j.bbr.2020.112917.
59. Berdugo-Vega, G., Lee, C.C., Garthe, A., Kempermann, G., and Calegari, F. (2021). Adult-born neurons promote cognitive flexibility by improving memory precision and indexing. Hippocampus *31*, 1068-1079. 10.1002/hipo.23373.
60. Kim, E.J., Ables, J.L., Dickel, L.K., Eisch, A.J., and Johnson, J.E. (2011). Ascl1 (Mash1) defines cells with long-term neurogenic potential in subgranular and subventricular zones in adult mouse brain. PLoS One *6*, e18472. 10.1371/journal.pone.0018472.
61. Castillon, C., Gonzalez, L., Domenichini, F., Guyon, S., Da Silva, K., Durand, C., Lestaevel, P., Vaillend, C., Laroche, S., Barnier, J.V., and Poirier, R. (2020). The intellectual disability PAK3 R67C mutation impacts cognitive functions and adult hippocampal neurogenesis. Hum Mol Genet *29*, 1950-1968. 10.1093/hmg/ddz296.
62. Sloviter, R.S., Dichter, M.A., Rachinsky, T.L., Dean, E., Goodman, J.H., Sollas, A.L., and Martin, D.L. (1996). Basal expression and induction of glutamate decarboxylase GABA in excitatory granule cells of the rat and monkey hippocampal dentate gyrus. The

Journal of Comparative Neurology *373*, 593-618. 10.1002/(sici)1096-9861(19960930)373:4<593::Aid-cne8>3.0.Co;2-x.

63. Perederiy, J.V., Luikart, B.W., Washburn, E.K., Schnell, E., and Westbrook, G.L. (2013). Neural injury alters proliferation and integration of adult-generated neurons in the dentate gyrus. J Neurosci *33*, 4754-4767. 10.1523/JNEUROSCI.4785-12.2013.

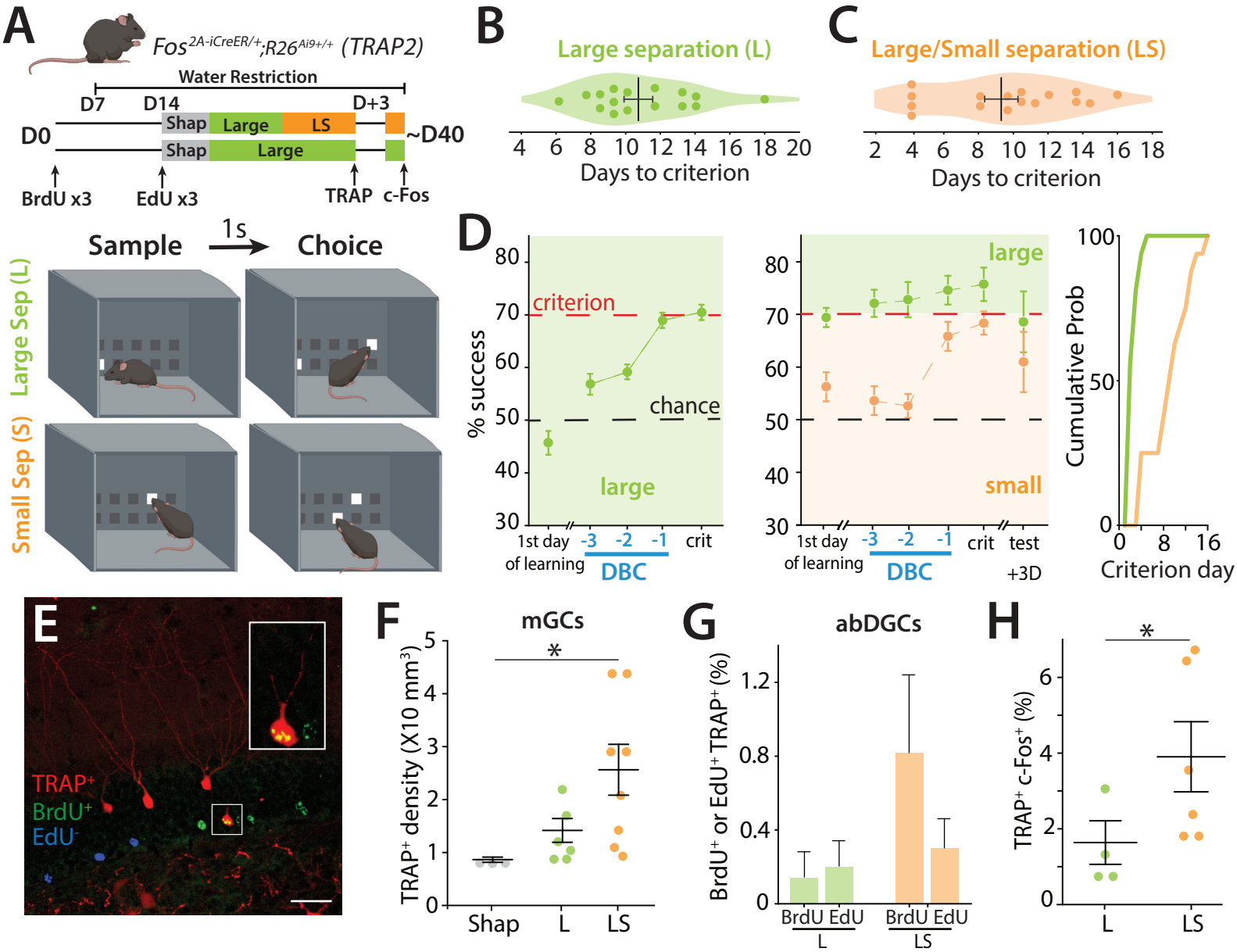
A
Fos2A-iCreER/+;R26Ai9+/+ (TRAP2)
Water Restriction
D7
D14
D+3
D0
Shap
Large
LS
~D40
BrdU x3
EdU x3
TRAP
c-Fos
Sample
1s
Choice
Large Sep (L)
Small Sep (S)
B
Large separation (L)
Days to criterion
C
Large/Small separation (LS)
Days to criterion
D
% success
criterion
chance
large
small
1st day of learning
DBC
crit
test +3D
Cumulative Prob
Criterion day
E
TRAP+
BrdU+
EdU-
F
mGCs
TRAP+ density (X10 mm3)
Shap
L
LS
G
abDGCs
BrdU+ or EdU+ TRAP+ (%)
BrdU EdU
H
TRAP+ c-Fos+ (%)

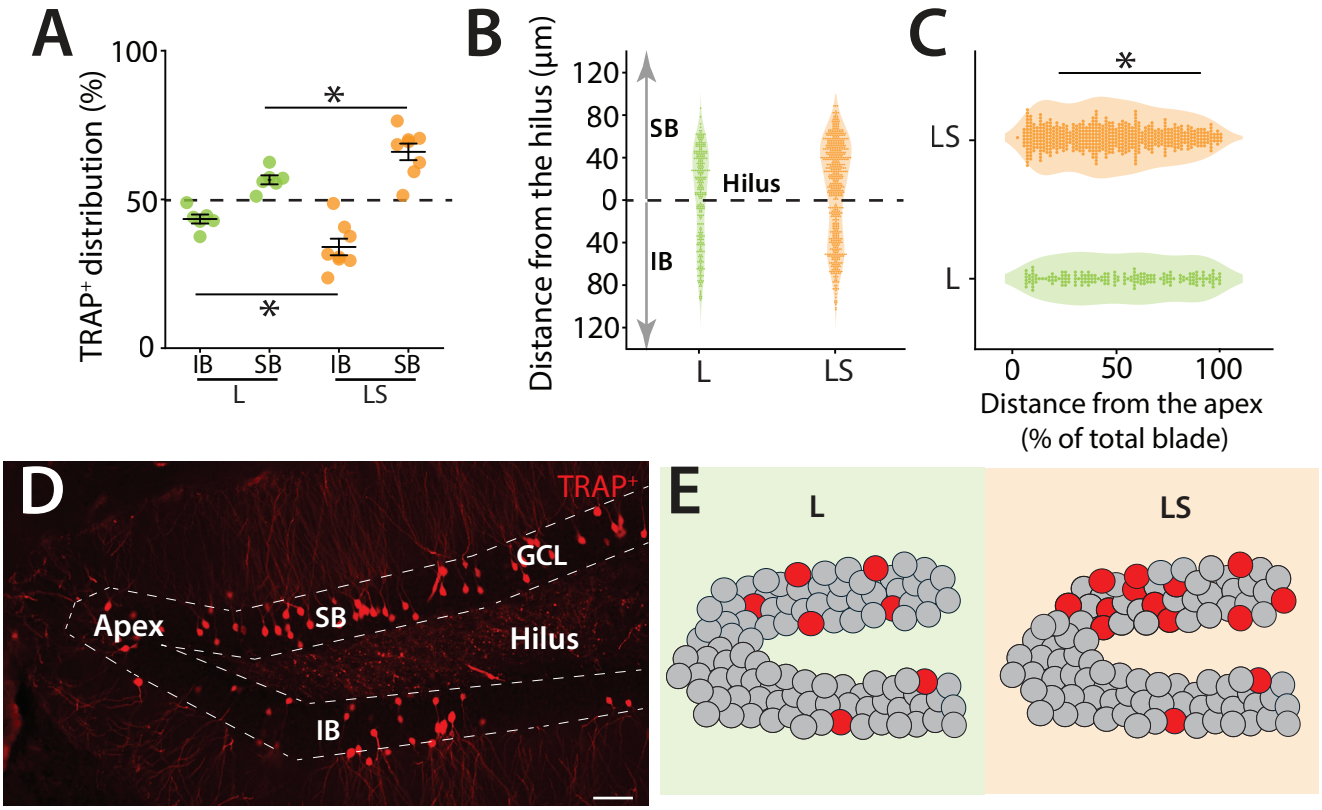
A
TRAP+ distribution (%)
100
50
0
*
*
IB
SB
IB
SB
L
LS
B
Distance from the hilus (µm)
120
80
40
0
40
80
120
SB
IB
Hilus
L
LS
C
*
LS
L
0
50
100
Distance from the apex
(% of total blade)
D
TRAP+
GCL
Apex
SB
Hilus
IB
E
L
LS

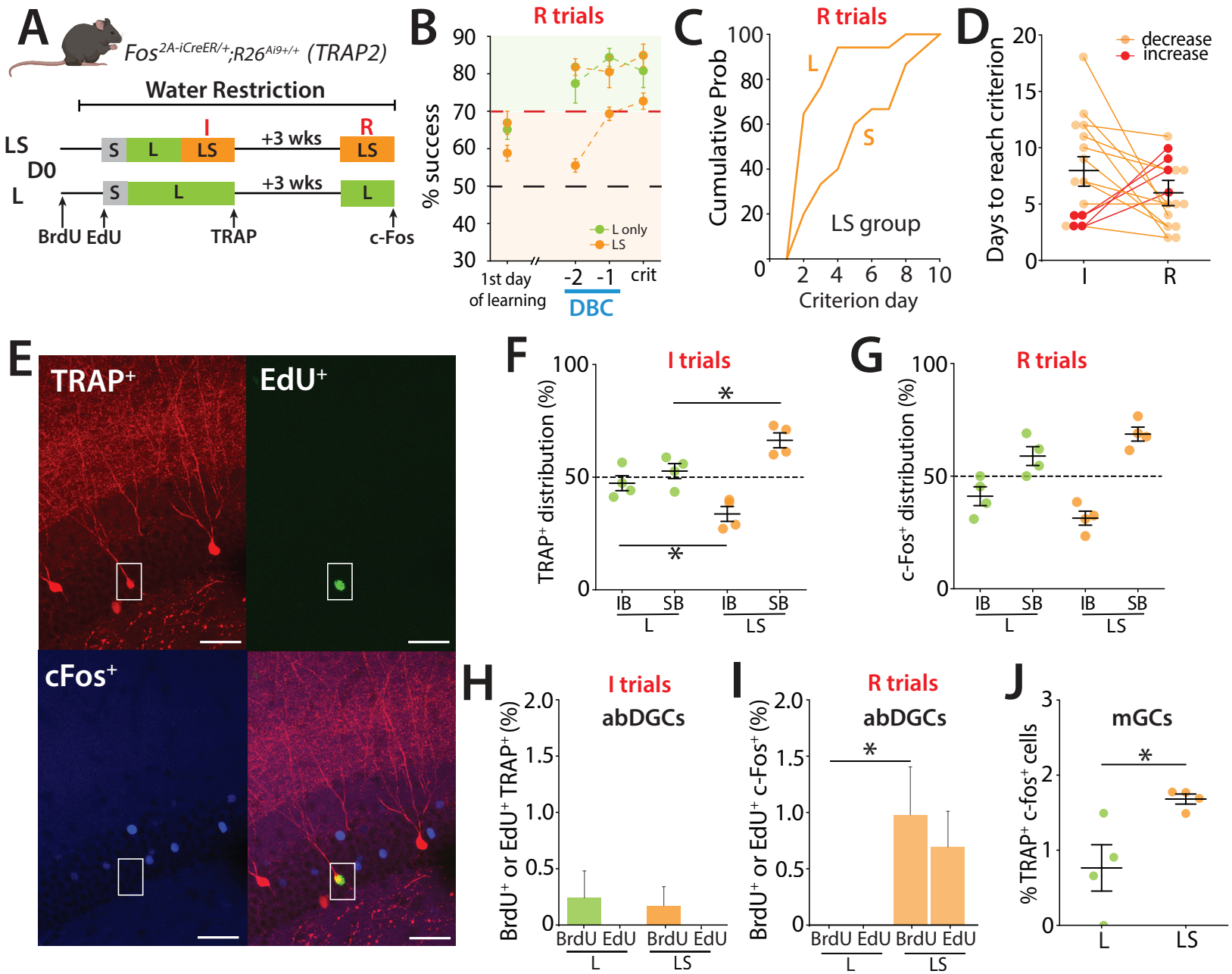
A
Fos2A-iCreER/+;R26Ai9+/+ (TRAP2)
Water Restriction
LS
D0
L
S
L
LS
I
+3 wks
R
LS
S
L
+3 wks
L
BrdU EdU
TRAP
c-Fos
B
R trials
% success
L only
LS
1st day of learning
-2
-1
crit
DBC
C
R trials
Cumulative Prob
L
S
LS group
Criterion day
D
decrease
increase
Days to reach criterion
I
R
E
TRAP+
EdU+
cFos+
F
I trials
TRAP+ distribution (%)
IB
SB
IB
SB
L
LS
G
R trials
c-Fos+ distribution (%)
IB
SB
IB
SB
L
LS
H
I trials
abDGCs
BrdU+ or EdU+ TRAP+ (%)
BrdU EdU
BrdU EdU
L
LS
I
R trials
abDGCs
BrdU+ or EdU+ c-Fos+ (%)
BrdU EdU
BrdU EdU
L
LS
J
mGCs
% TRAP+ c-fos+ cells
L
LS

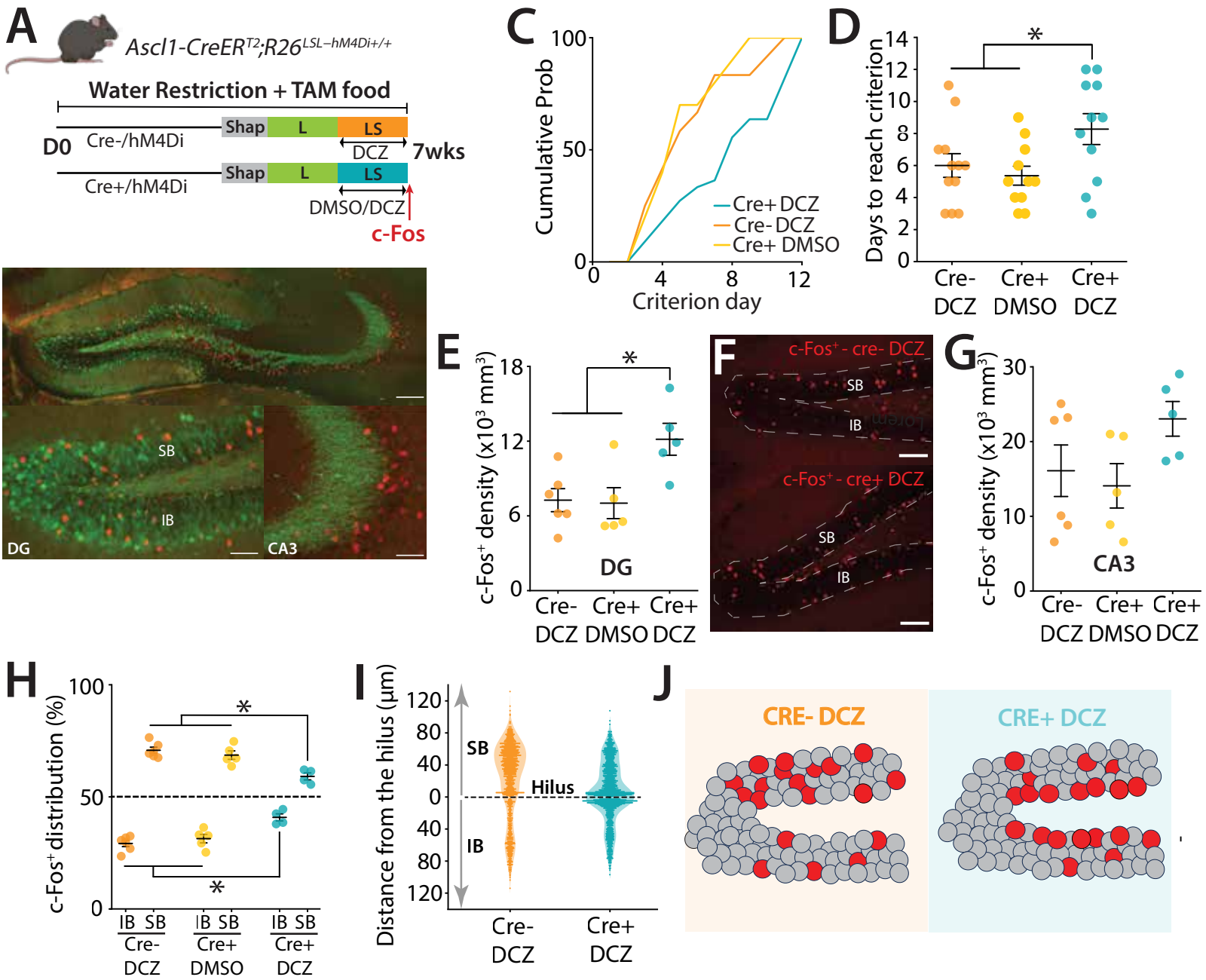
A
Ascl1-CreER^{T2};R26$^{LSL-hM4Di+/+}$
Water Restriction + TAM food
D0
Cre-/hM4Di
Shap
L
LS
DCZ
7wks
Cre+/hM4Di
DMSO/DCZ
c-Fos
SB
IB
DG
CA3
C
Cumulative Prob
Criterion day
Cre+ DCZ
Cre- DCZ
Cre+ DMSO
D
Days to reach criterion
Cre- DCZ
Cre+ DMSO
Cre+ DCZ
E
c-Fos+ density (x10³ mm³)
DG
F
c-Fos+ - cre- DCZ
c-Fos+ - cre+ DCZ
G
CA3
H
c-Fos+ distribution (%)
IB SB
I
Distance from the hilus (µm)
Hilus
J
CRE- DCZ
CRE+ DCZ

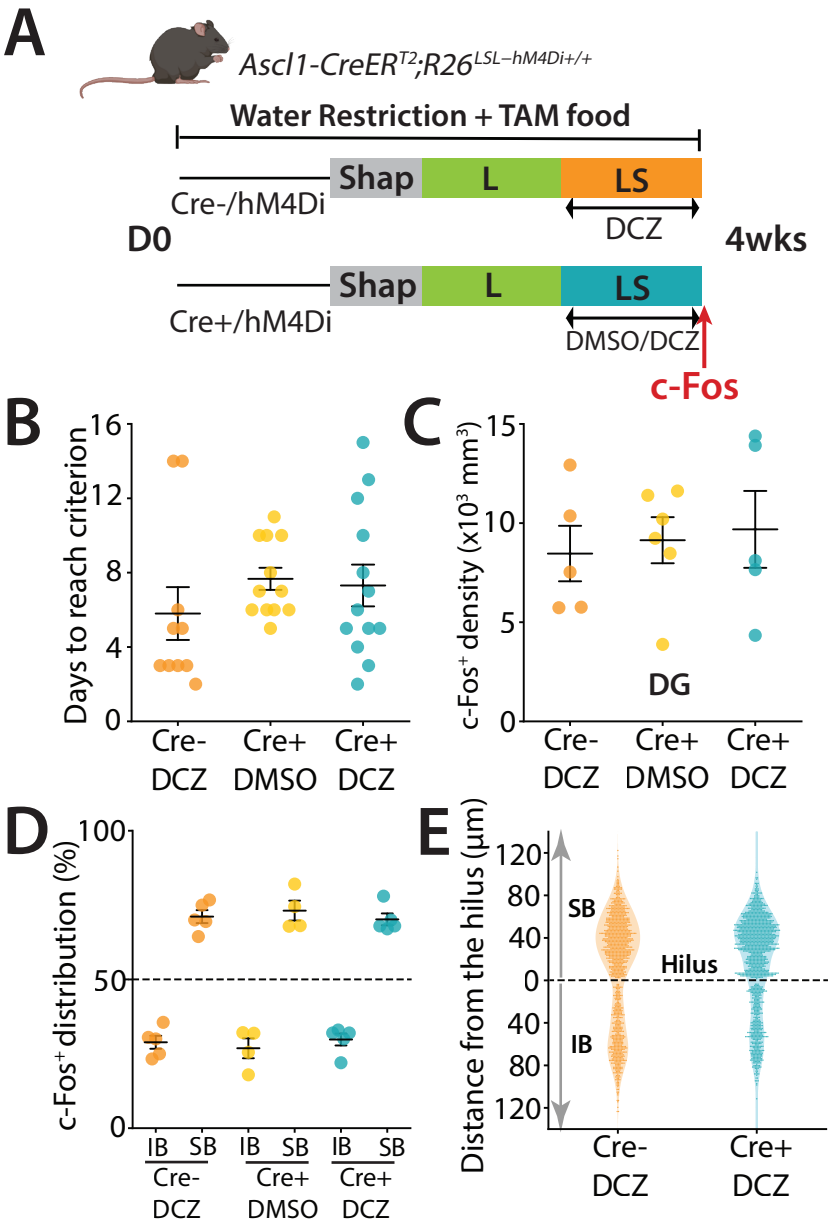
A
Ascl1-CreER^{T2};R26$^{LSL-hM4Di+/+}$
Water Restriction + TAM food
Shap
L
LS
Cre-/hM4Di
DCZ
D0
4wks
Shap
L
LS
Cre+/hM4Di
DMSO/DCZ
c-Fos
B
Days to reach criterion
16
12
8
4
0
Cre-
DCZ
Cre+
DMSO
Cre+
DCZ
C
c-Fos$^+$ density (x10^3 mm^3)
15
10
5
0
DG
Cre-
DCZ
Cre+
DMSO
Cre+
DCZ
D
c-Fos$^+$ distribution (%)
100
50
0
IB
SB
IB
SB
IB
SB
Cre-
DCZ
Cre+
DMSO
Cre+
DCZ
E
Distance from the hilus (µm)
120
80
40
0
40
80
120
SB
Hilus
IB
Cre-
DCZ
Cre+
DCZ

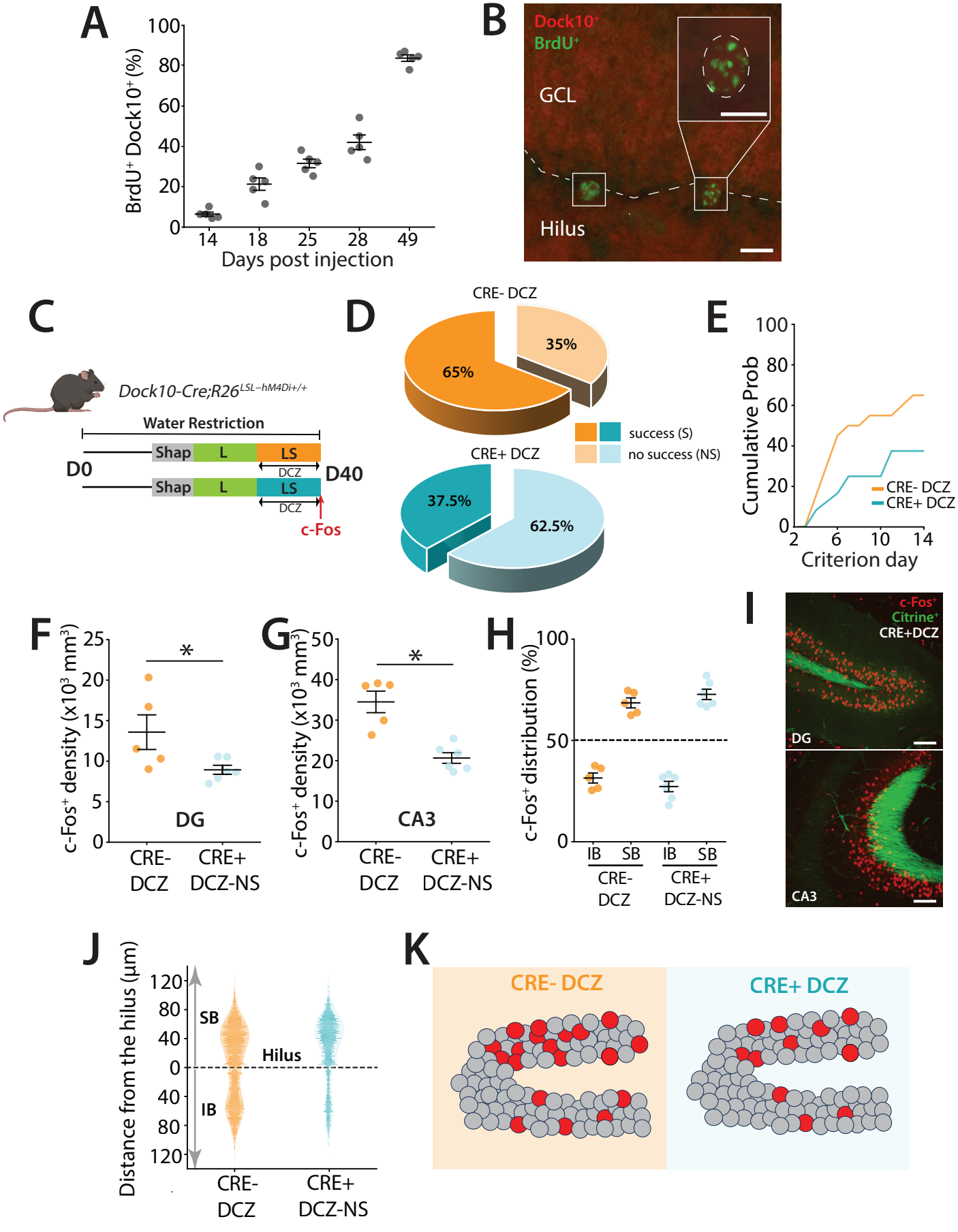
A
BrdU+ Dock10+ (%)
100
80
60
40
20
0
14
18
25
28
49
Days post injection
B
Dock10+
BrdU+
GCL
Hilus
C
Dock10-Cre;R26LSL−hM4Di+/+
Water Restriction
Shap
L
LS
DCZ
D0
D40
c-Fos
D
CRE- DCZ
65%
35%
success (S)
no success (NS)
CRE+ DCZ
37.5%
62.5%
E
Cumulative Prob
Criterion day
CRE- DCZ
CRE+ DCZ
F
c-Fos+ density (x10³ mm³)
DG
CRE- DCZ
CRE+ DCZ-NS
G
CA3
H
c-Fos+ distribution (%)
IB
SB
I
c-Fos+
Citrine+
CRE+DCZ
DG
CA3
J
Distance from the hilus (µm)
SB
IB
Hilus
K
CRE- DCZ
CRE+ DCZ

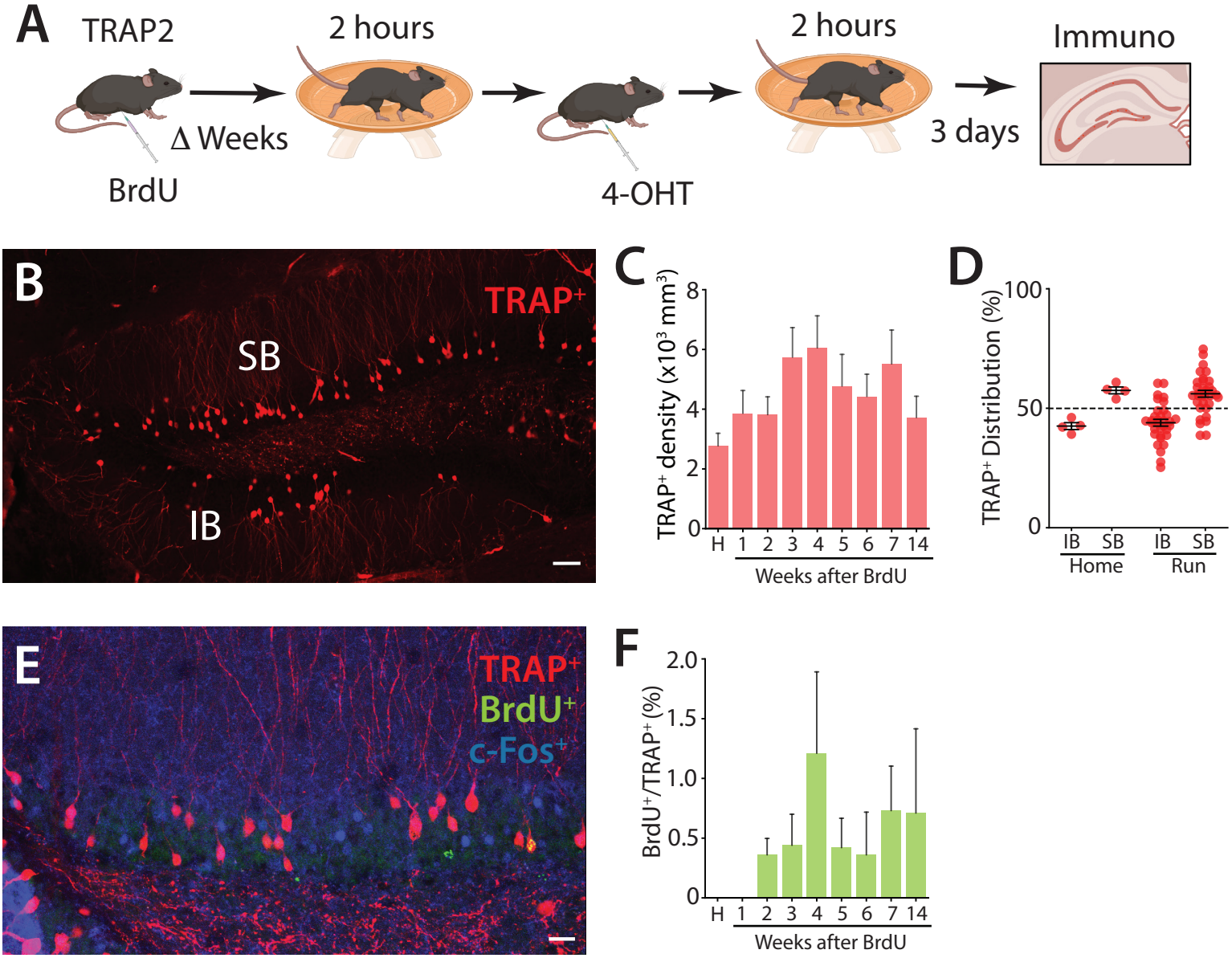
A
TRAP2
2 hours
2 hours
Immuno
Δ Weeks
3 days
BrdU
4-OHT
B
TRAP+
SB
IB
C
TRAP+ density (x10³ mm³)
8
6
4
2
0
H 1 2 3 4 5 6 7 14
Weeks after BrdU
D
TRAP+ Distribution (%)
100
50
0
IB SB IB SB
Home Run
E
TRAP+
BrdU+
c-Fos+
F
BrdU+/TRAP+ (%)
2.0
1.5
1.0
0.5
0
H 1 2 3 4 5 6 7 14
Weeks after BrdU

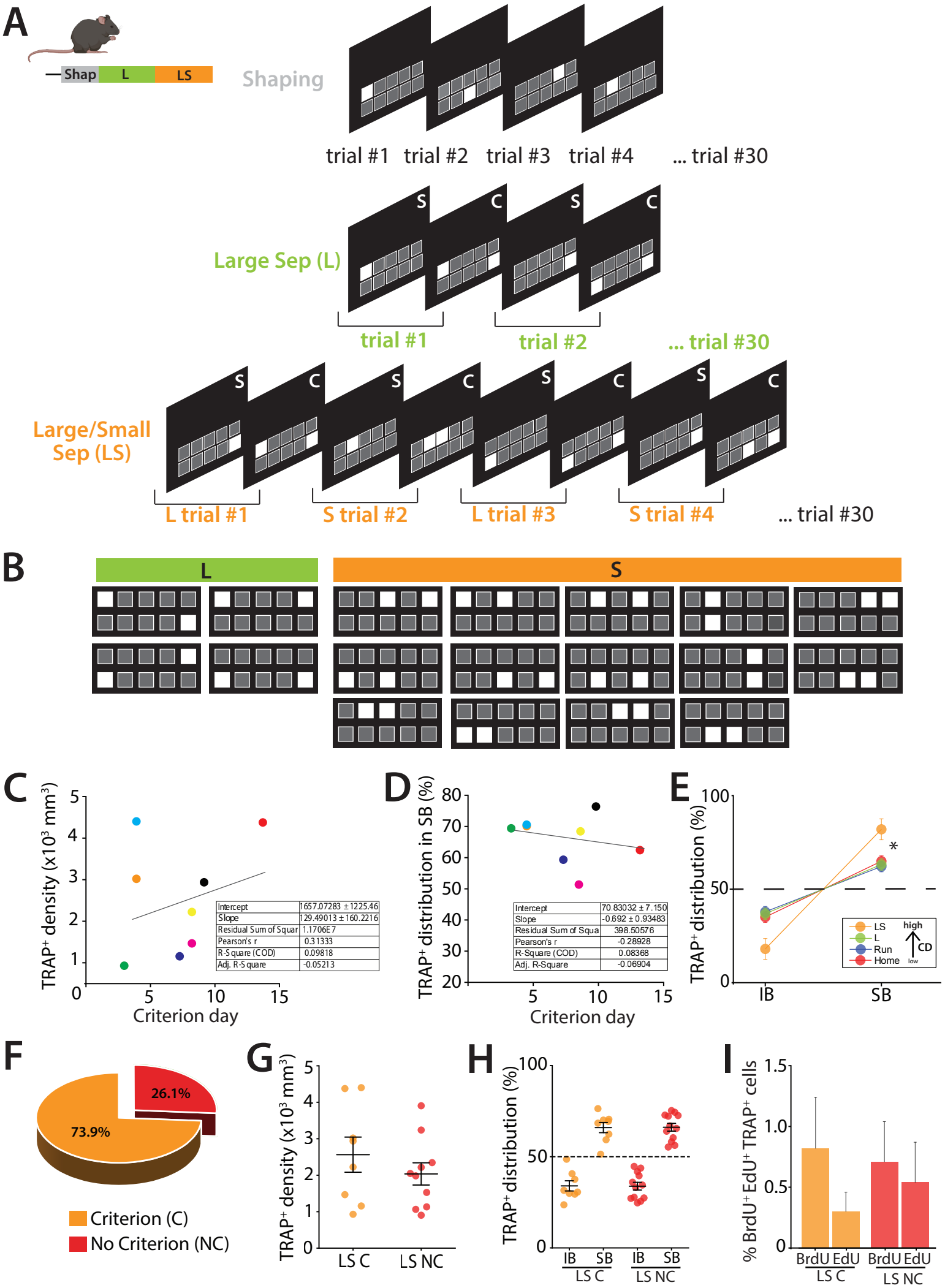
A
Shap
L
LS
Shaping
trial #1
trial #2
trial #3
trial #4
... trial #30
Large Sep (L)
S
C
trial #1
trial #2
... trial #30
Large/Small Sep (LS)
L trial #1
S trial #2
L trial #3
S trial #4
... trial #30
B
L
S
C
TRAP+ density (x10³ mm³)
Criterion day
Intercept 1657.07283 ± 1225.46
Slope 129.49013 ± 160.2216
Residual Sum of Squar 1.1706E7
Pearson's r 0.31333
R-Square (COD) 0.09818
Adj. R-Square -0.05213
D
TRAP+ distribution in SB (%)
Criterion day
Intercept 70.83032 ± 7.150
Slope -0.692 ± 0.93483
Residual Sum of Squa 398.50576
Pearson's r -0.28928
R-Square (COD) 0.08368
Adj. R-Square -0.06904
E
TRAP+ distribution (%)
IB
SB
LS
L
Run
Home
high
CD
low
F
26.1%
73.9%
Criterion (C)
No Criterion (NC)
G
TRAP+ density (x10³ mm³)
LS C
LS NC
H
TRAP+ distribution (%)
IB
SB
LS C
LS NC
I
% BrdU+ EdU+ TRAP+ cells
BrdU
EdU
LS C
LS NC

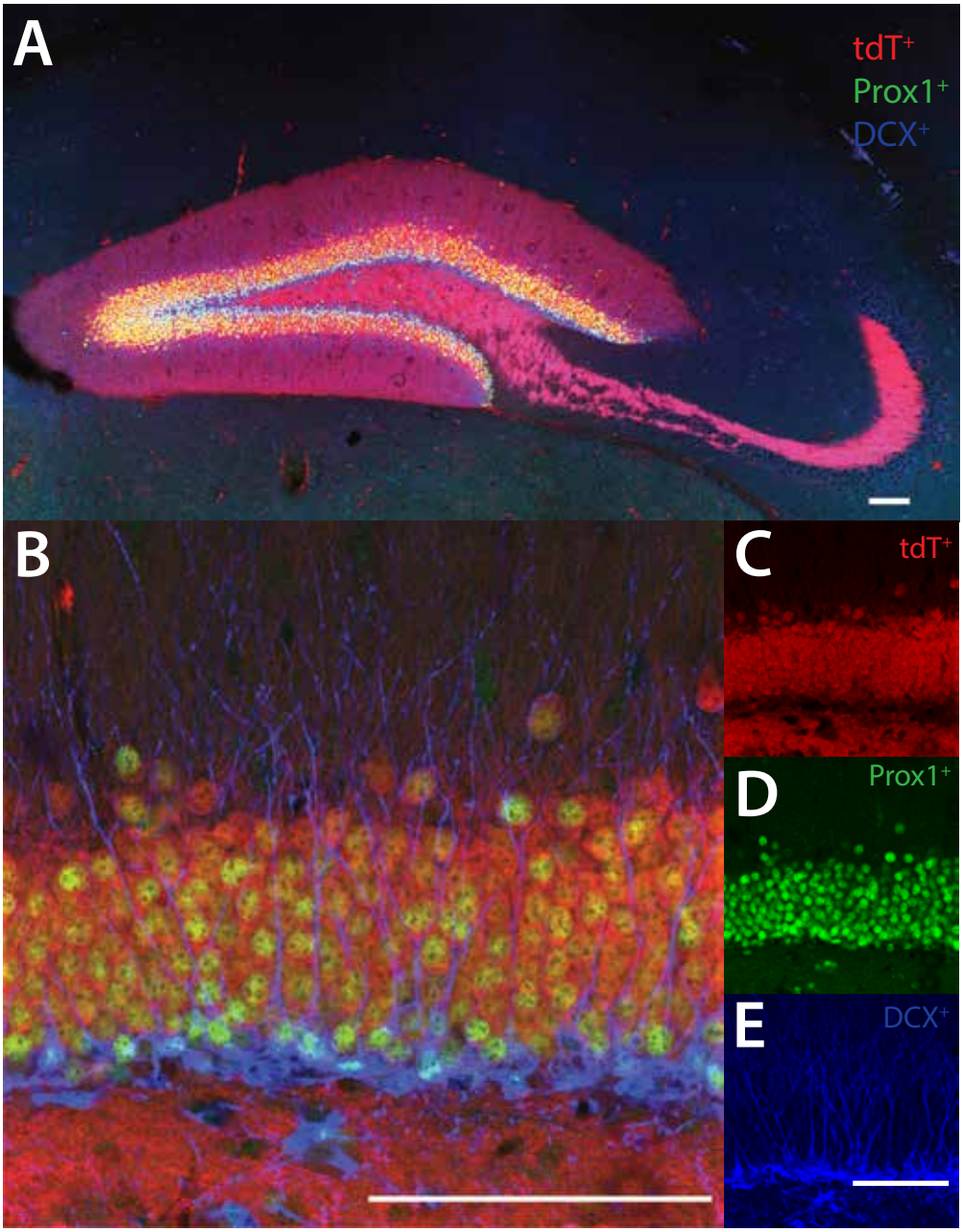
A
tdT+
Prox1+
DCX+
B
C
tdT+
D
Prox1+
E
DCX+